Chapter IV. Realistic microstructures

Introduction

A polycrystal consists of GBs differently oriented with respect to each other and the diffusion direction. Even though it is important to take these orientations into account, conventional GB diffusion models ignore this effect. In this chapter realistic microstructures are discussed, and the conventional analysis is applied to the diffusion profiles calculated in both the B-regime and the A-regime. The influence of the crystallographic misorientations of the grains is neglected [Lea57].

It is important to mention that the reliability of the model of isolated boundaries (fig. 1.2) as a representation of a polycrystal is partly based on sufficiently small values of the parameter β (see discussion below and [Kau95]) and/or large grain sizes. In this case the grain shape and the GBs orientations do not play a significant role. On the other hand, as the diffusion time (t) shortens, the diffusion process in a polycrystal is mostly determined by the GB contribution. This is the typical situation in materials with small grain sizes.

Different theoretical methods were recently applied in order to analyze the diffusion behavior under realistic conditions. Attempts were undertaken to analyze GB diffusion in realistic microstructures by using Potts model [Swi97] and phase field approach [Zhu01]. Moreover, attempts were also undertaken to obtain some analytical solutions to describe diffusion in real polycrystals [Bed05]. However, the model of parallel boundaries (the same as the isolated boundary model in the B-regime) and the model of square grains are very often considered when simulating diffusion in polycrystalline materials by using the Monte-Carlo method [Bel03]. Also the model of spherical grains is convenient for analytical evaluations [Harr61] as well as for numerical considerations [Sak90]. The analysis of GB diffusion in realistic microstructures is mostly restricted to the extreme cases of the A- or C-regime. Consequently, both the model of parallel boundaries and the model of square grains are analyzed in the present study in the B- as well as A-regime but with an eye to more realistic (general) microstructures, developed here by using the finite element approach. Further literature and ideas on simulating diffusion in the realistic microstructures are discussed in the following sections.

4.1 Finite Element Calculation. To get started

As already mentioned the finite element method (FEM) is a very useful tool for studying different physical processes [Sim06]. Application of the FEM to problems of diffusion and heat conduction was discussed in the literature due to the importance of these processes and the possibility to model these by means of classical differential equations (for example, [Com94]). That is, a linear partial differential equation of the second order of parabolic type is treated in the case of mass transfer (heat conduction) [Wei65]. Moreover, a numerical study of such processes can serve as a model simulation of instationary problems for the finite element calculations. However, problems such as GB diffusion have never been studied intensively by FEM. The paper of Whipple [Whi54] was published in earlier 50‘s of the last century. Since that time, Whipple’s solution has been remaining the only exact solution of diffusion equations to the GB diffusion problem, and there was no need to solve the Fisher system by means of numerical methods. Only a single paper, by Z. Knesl *et al.* [Kne74], was dealing with FEM for interacting GBs in the model of square grains. Even though, numerical methods can help to obtain the concentration distribution for such geometrical situations. As a result of this simulation they simply compared the diffusion profiles obtained for the isolated boundary model to those for the square grains for the

interacting GBs. Despite this fact, it was a pioneering work as regards on the application of FEM to the problems of GB diffusion.

There is always a numerical aspect relating to the integration of differential equations. The accuracy of integration defines the quality of simulating concentration profiles, which is reflected in the parameters obtained from simulated profiles. The integration can become very critical in the cases of extremely small diffusion lengths, because the diffusion process in the bulk (grain) is concentrated closely to the surface where the gradients are very high. This is specifically important for GB diffusion, because of two interrelated processes: the GB diffusion rates can be significantly different from the bulk diffusion rates. The GB contribution to the overall process is prolonged along the y-coordinate (fig. 1.2) at short t and is strongly concentrated around the GB. This implies that high densities of integration meshes are required in those regions in order to get accurate results. Otherwise, the simulated diffusion profiles could either be inaccurate or even physically inadequate by giving negative concentrations. It is the purpose here to show: 1) how the GB diffusion problem can be resolved by using FEM, 2) which problems arise when integrating Fisher's system (Eq. (1.6a)) by FEM, 3) what conclusions can be drawn from numerical analysis.

4.1.1 Main characteristics of the geometrical model of isolated boundary used in the finite element program

The typical t used in the present work is 2000 s for $\Delta = 2.2 \cdot 10^4$. In this case $L_g \approx 0.77$ nm, i.e. it is comparable with the interatomic spacing, whereas $L_{gb} \approx 64.61$ nm. Let the whole length of geometrical model be 500 nm and the width 40 nm. The length of 500 nm is mostly used, if not stated otherwise. That is, the geometry is represented by a rectangle box with the diffusant applied at the free surface. The diffusant moves into the box under the concentration gradient until a whole space is filled up by the diffusant. This problem is again two-dimensional with reflecting boundaries at all sides of the geometrical model, if a special property is not defined, for example, the GB or the free surface. The GB thickness (δ) is neglected as it is supposed by Fisher's model. The latter means that the GB is represented by a line with neglecting the GB concentration within it. The relevant geometrical model is equivalent to that used to integrate Whipple's solution. The only difference between the two solutions is the influence of reflecting boundaries in the FEM model. Consequently, Eq. (1.3a) should be added by the zero-flux condition at the bottom of geometry. However, our main analysis is related to the maximum of the derivative of $\ln C_{av} = f(y^{6/5})$. If the maximum is not

affected by the boundary, the solution is valid for infinite systems as well. The role of this condition for simulation of diffusion in the A-regime is discussed in section 4.2.3.1.

4.1.2 A comparison of Whipple's solution and FLUX-EXPERT's simulation results

To compare Whipple's solution with FLUX-EXPERT's result, a consideration of single GB is necessary. The two results are shown in fig. 4.1. These coincide within an error of 1% until the influence of the zero-flux boundary condition becomes significant at larger coordinates (the derivative goes to zero). This demonstrates that the model applied in FLUX-EXPERT (the geometrical model, mesh as well as the derived Eq. (2.8)) can be used to integrate the Fisher system. This is particularly important because diffusion is studied here under extreme conditions: short t and diffusion lengths, leading to high derivatives. In the next sections the results of the integration in FLUX-EXPERT for different geometrical models and parameters are discussed. All these results were obtained with a very high accuracy, what is, however, computationally costly.

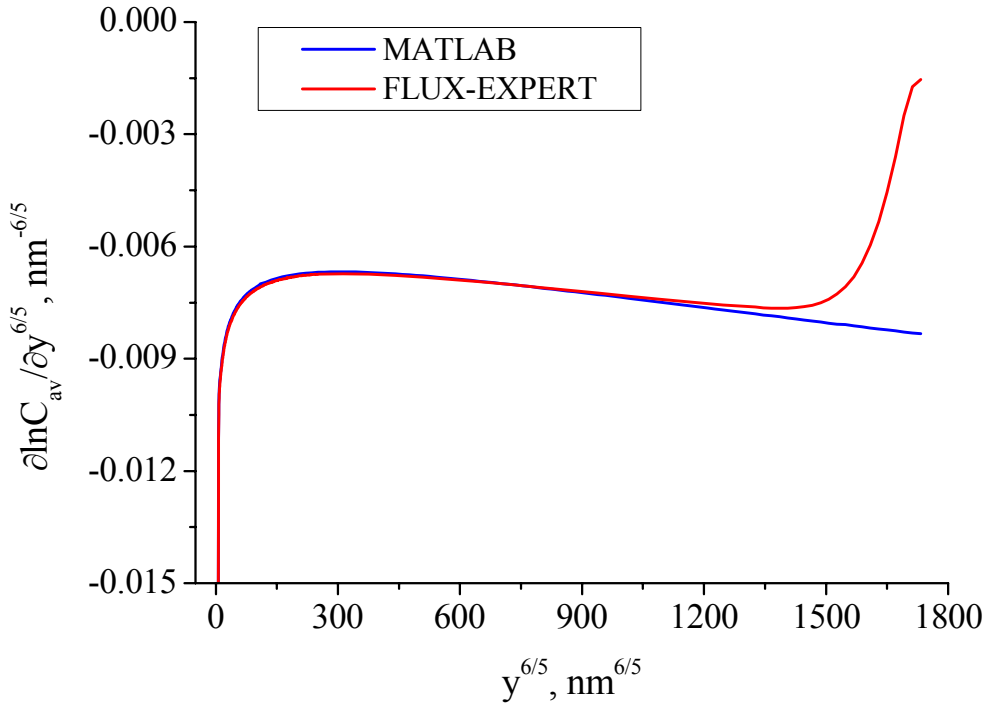

Fig. 4.1 A comparison of the integration by FEM (FLUX-EXPERT) with Whipple's solution (MATLAB). The ratio $\Delta = 2.2 \cdot 10^4$ and t = 2000 s.

4.1.3 The accuracy of results obtained in FLUX-EXPERT

4.1.3.1 The averaging of concentration C_g

It is reasonable to discuss here how, using FLUX-EXPERT, the concentration $C_g(x, y, t)$ is integrated along the direction perpendicular to the GB. The diffusion parameters are found from the profile of concentration $C_g(x, y, t)$ averaged along the x-direction (fig. 1.2), which reveals the concentration $C_{av}(y, t)$ as a function of coordinate y only. This is done in the same manner as in real diffusion experiments by using, for example, tracer measurements [Ask70]. FLUX-EXPERT gives the concentration distribution over all mesh points. One can also plot the concentration along different paths of the geometrical model [Flu92e]; however, the averaging is not realized in the program specifically. The special script was written by using the programming language Perl in order to obtain C_{av}.

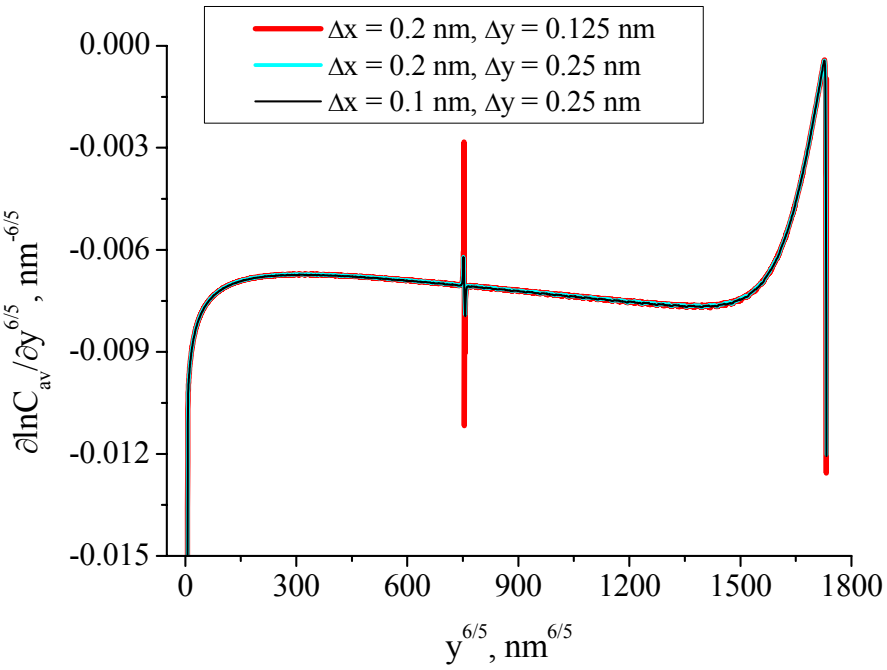

Fig. 4.2 Variation of the derivative $\partial \ln C_{av}/\partial y^{6/5}$ with $y^{6/5}$ calculated with different intervals Δx and Δy.

The script runs the module XPLOIT [Flu92e], in which the concentration is calculated along the paths of constant y-coordinates in the automatic mode. The module allows one to calculate the integral itself; however the averaging is done by dividing that integral by $(x_{max} - x_{min})$, i.e. the width of the geometrical model used. Consequently,

$$C_{av}(y,t) = \frac{1}{x_{max} - x_{min}} \int_{x_{main}}^{x_{max}} C_g(x,y,t)dx \qquad (4.1)$$

The steps of integration are controlled in this script along both directions, but the interval along the x-direction (Δx) is, of course, an important parameter. In the present work the only intervals used to obtain C_{av} are Δx = 0.20 and 0.25 nm. If the interval Δx is decreased, say by a factor of 2, the derivative does not change and, in principle, the same result can be obtained (fig. 4.2, black line). The step along the y-direction can influence the result as well, leading to numerical instabilities similar to those observed by integrating Whipple's solution (see section 3.2). The instability is reflected in noise and spikes, for example at $y^{6/5} \sim 750$ $nm^{6/5}$ in fig. 4.2. Such spikes are enhanced when the interval Δy decreases.

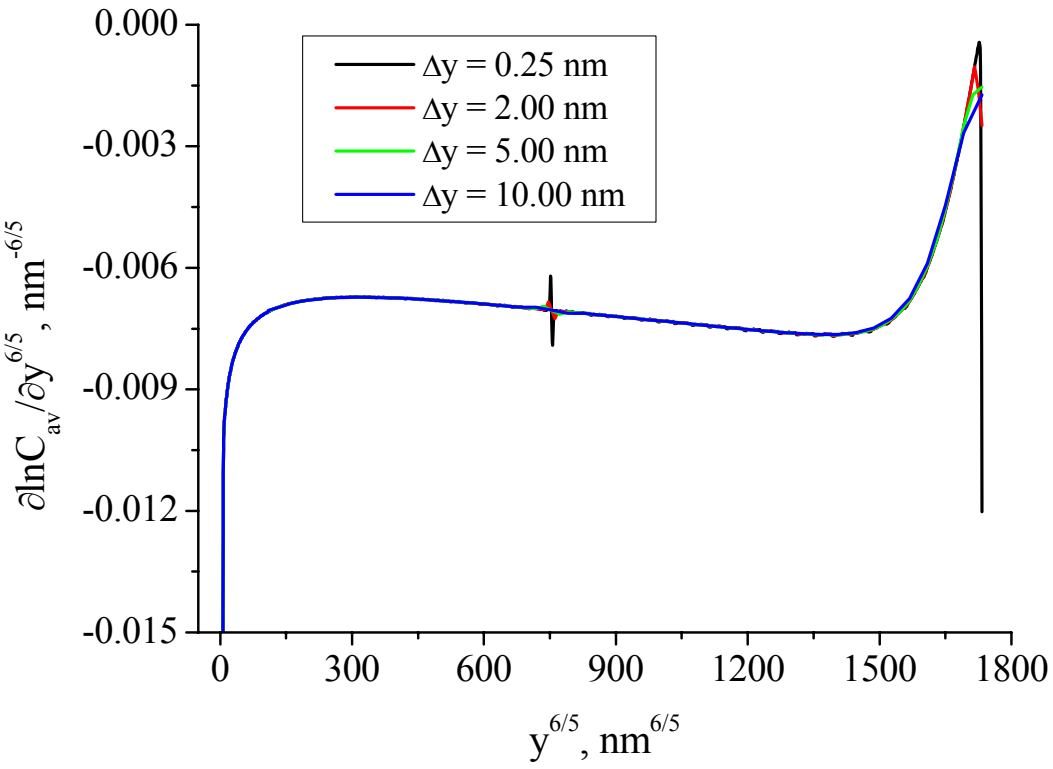

Fig. 4.3 Variation of the derivative $\partial \ln C_{av}/\partial y^{6/5}$ with $y^{6/5}$ calculated with different steps Δy in the GB part.

Consequently, the following Δy-intervals were tested in the GB part of the diffusion profiles (i.e. in the region 50 – 500 nm for $\Delta = 2.2 \cdot 10^4$ at t = 2000 s): 0.25, 2.00, 5.00, and 10.00 nm, while the interval in the bulk part of the profile was fixed to 0.25 nm. The derivatives of the corresponding diffusion profiles are presented in fig. 4.3. In this way one

can show that increasing the interval of integration (Δy) in the GB part leads to derivatives without instabilities. In order to get a similarly smooth profile of the derivative three steps were finally adapted according to three parts of the diffusion profile: bulk part, GB part and the reflecting boundary. The example of this profile is shown in fig. 4.1 obtained with the Δy-steps 0.25, 20.0, 5.0 in the bulk, GB and reflecting boundary parts, respectively.

4.1.3.2 The effect of the finite element mesh

Diffusion has a specific feature which should be taken into account for numerical integration of the diffusion equations by FEM. The diffusion gradients vary with time striving for zero until the equilibrium is achieved. On simulating diffusion in different kinetic regimes, the problem of the mesh becomes very important. One would thus presume different density meshes in different parts of geometry and/or at different t. This also complicates the numerical integration of diffusion equations. However, it would be useful to find a universal mesh for certain diffusion parameters, sufficiently dense to use it under different conditions. Moreover, there is always a trade-off between mesh density and time interval (Δt). Several calculations are typically needed to get a final diffusion profile, which depends on the parameters (diffusivities, t) used in the numerical experiment. Unfortunately, it is not possible to simply increase the density, because it would giantly increase the computational time. Moreover, the finite element program used has limits too. In particular, FLUX-EXPERT has a maximum number of elements of one million (!), at least for the version of the program used in the present work [Flu00]. One can imagine that this maximum number is fixed for the whole geometry, and once the geometry was defined, satisfying the accuracy, it is not possible to increase its length further. One should pay attention that these numerical problems become specifically important when simulating diffusion in nanocrystalline materials due to small diffusion lengths.

The mesh density for the concentration profile plotted in fig. 4.1 is as follows: 0.25 nm along the x-direction and about 0.24 nm along the y-direction. Hereafter this mesh is called mesh 1. Such a mesh density implies the number of triangle elements to be 657729 for the geometry of 40 nm in width and 500 nm in length (40x500 nm^2). The same density for the geometry of 25 nm in width gives 409940 triangle elements. This is the most dense mesh used in the present work (except the space charge layer problems discussed in the next chapter), for which the number of elements is already half of the program's limit (see also other examples in table 4.1). The result obtained by using this mesh is consistent with that obtained by

integrating Whipple's solution (fig. 4.1). This allows mesh 1 to be a model mesh and to skip a comparison of that with more dense meshes. In fig. 4.4a the profile for mesh 1 (red curve) is compared with that for smaller number of elements. The density was also decreased to 0.5 nm and about 0.48 along the x- and y-direction, respectively. This is a mesh, called mesh 2, with ~164884 elements for the sample: 40x500 nm^2. It is very important to note that for a mesh of smaller density the reflecting boundary leads to larger values of the concentration $C_{av}(y, t)$, especially at deeper y-coordinates. In this case the derivative looks more like a straight line in the GB part artificially, but this is purely the effect of the mesh only (green and blue lines in fig. 4.4a). In the worst case, the decrease of the mesh density could lead to a vanishing of the GB part, affecting the maximum so strongly that the slope of the diffusion profile could not be obtained.

The integration parameters (the interval Δy, see discussion above) differ for both mesh 1 and mesh 2. The interval $\Delta y = 10$ nm and smaller along the GB part leads to the instabilities for mesh 2 (blue and green curves). In fig. 4.4b the comparison of mesh 1 is made with additional new meshes for the same geometry (40x500 nm^2) at longer t in order to get a preliminary impression of the introduced errors. Additionally, decreasing mesh density does not really allow one to start the calculation with short time of 200 s, as it was done with mesh 1. Consequently, the starting times are 200 s for mesh 3 and 7000 s for mesh 4 (table 4.1). In fig. 4.4b the noise (green curve) is related to a very small step integration Δy of 0.25 nm. Obviously, such intervals together with small densities are not advisable. The results for mesh 1 and mesh 3 coincide at t = 10700 s, demonstrating that one can use the meshes of smaller densities for simulating diffusion at higher t only. However, the main choice is made for mesh 1 is preferred as satisfying the necessary accuracy at short t and allowing t to be increased as well as the ratio of diffusivities (Δ).

Table 4.1 Parameters of different test meshes.

Name	Density along x/y direction	Number of triangle elements (40x500 nm^2)
mesh 1	0.25/0.24	657729
mesh 2	0.50/0.48	~164864
mesh 3	1.00/0.97	41391
mesh 4	2.00/1.95	10445

4.1.3.3 The effect of the time interval

a)

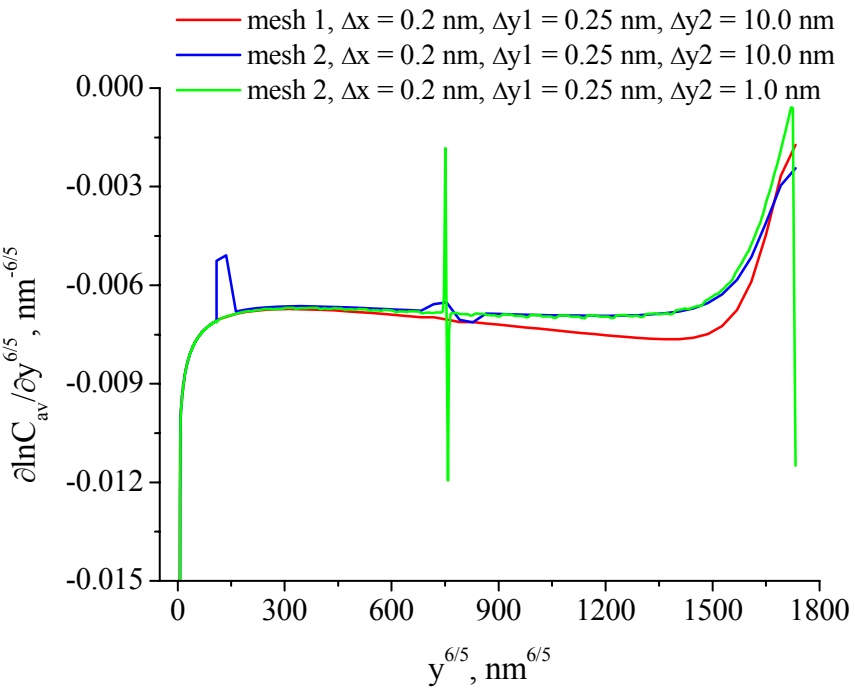

b)

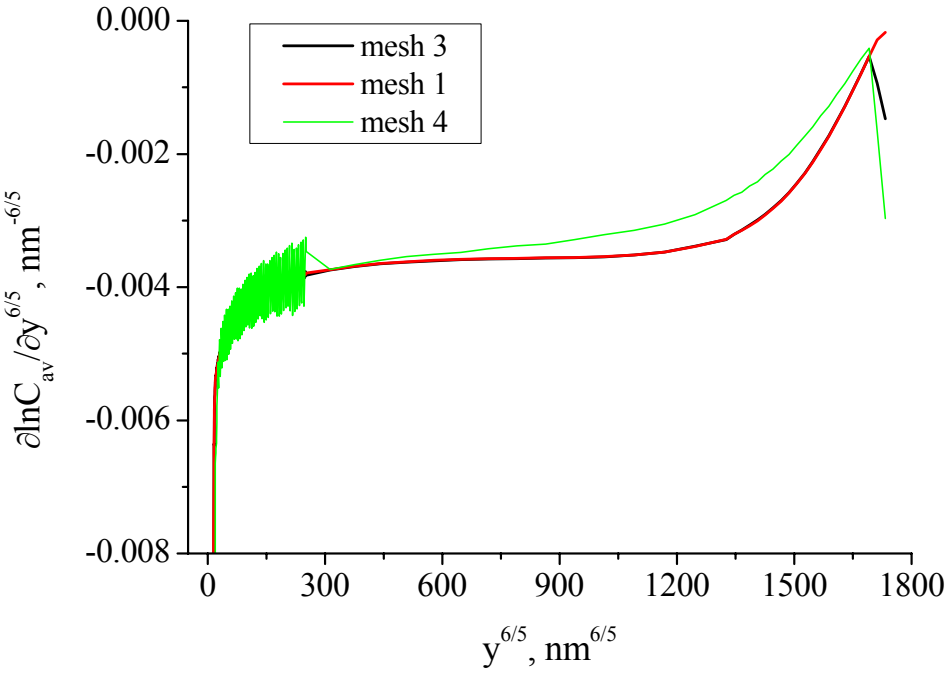

Fig. 4.4 A comparison of different meshes at a) t = 2000 s and b) t = 10700 s. The steps Δy1 and Δy2 mean the intervals in the bulk part and GB part of the profile, respectively.

As we deal with transitory problems, the solution strongly depends on the time interval used. The smaller the interval Δt the more accurate the solution. Because very small values Δt leads to time-consuming calculations, an appropriate computational procedure should be found with respect to that parameter too. In order to check its effect, various Δt were used, simulating the diffusion profile for conditions $\Delta = 2.2 \cdot 10^4$ at t = 2000 s. The interval Δt was varied from 600 s to 6.25 s, starting the calculation with t of 200 s. In all the calculations under conditions of the type-B kinetics (see section 1.2), this starting time was taken as 200 s, if not otherwise stated. Consequently, the largest Δt suggests 3 computational steps, whereas the smallest one 288 steps.

The profiles for various Δt are presented in fig. 4.5. One can see that there is a very little difference in the derivatives calculated for Δt = 6.25, 12.5 and 25 s. Finally, Δt = 12.5 s was used in all the calculations up to 13200 s. It was observed, that after 13200 s Δt can be increased and, consequently, in the A-regime the time interval of 20000 s was used.

The starting time value can affect the accuracy of a particular result, especially at very short t. That is why, Δt should be tuned every time, beginning a new calculation with a new geometry (or mesh) and parameters. In fig. 4.5 it is demonstrated that large Δt = 600 s leads to the vanishing of the maximum. Fitting the corresponding profile by a straight line does not give a correct slope.

4.2 Realistic polycrystalline microstructures

In GB diffusion studies the isolated boundary model (fig. 1.2) has been serving as a good approximation of a real microcrystalline structure for many years. However, a real microcrystalline structure comprises many GBs differently oriented to each other and to the diffusion direction. Ignoring the GBs orientations seems justified by the fact that in coarse-grained materials the influence of a GB orientation on a concentration profile is negligible, because of the possibility to study diffusion under conditions of high temperatures and/or long t. The type-B kinetics is considered for the coordinate developing process. In the case of coarse-grained materials L_{gb} is also less than d [Kau95], i.e. the condition given by Eq. (1.11a) is fulfilled. It is believed that the diffusion process changes with time and along a GB oriented perpendicularly to the surface. One would expect that the role of GBs, which are not parallel to the diffusion direction increases, if the β-parameter increases (Eq. (1.9d)), i.e. the larger ratio Δ or significantly shorter t (and/or smaller d) are considered. The former would lead to the condition $L_{gb} >> d$, whereas the latter tends to the specific type-B kinetics in which all the

properties discussed so far are valid (chapter III) and the condition $L_{gb} >> d$ can be recalled also. Interestingly, L_g can reach d earlier than L_{gb}, what would exactly mean that one faces the type-B_4 kinetics (fig. 1.5a, imagine that d > 25 nm) but this is only possible for coarse-grained materials.

There is another interesting finding of Mishin [Mis92b] that plotting the diffusion profile versus $y^{6/5}$ or simply y gives, in principle, similar errors of determining D_{gb} in a coarse-grained polycrystal when only the orientation of a GB to the surface is taken into

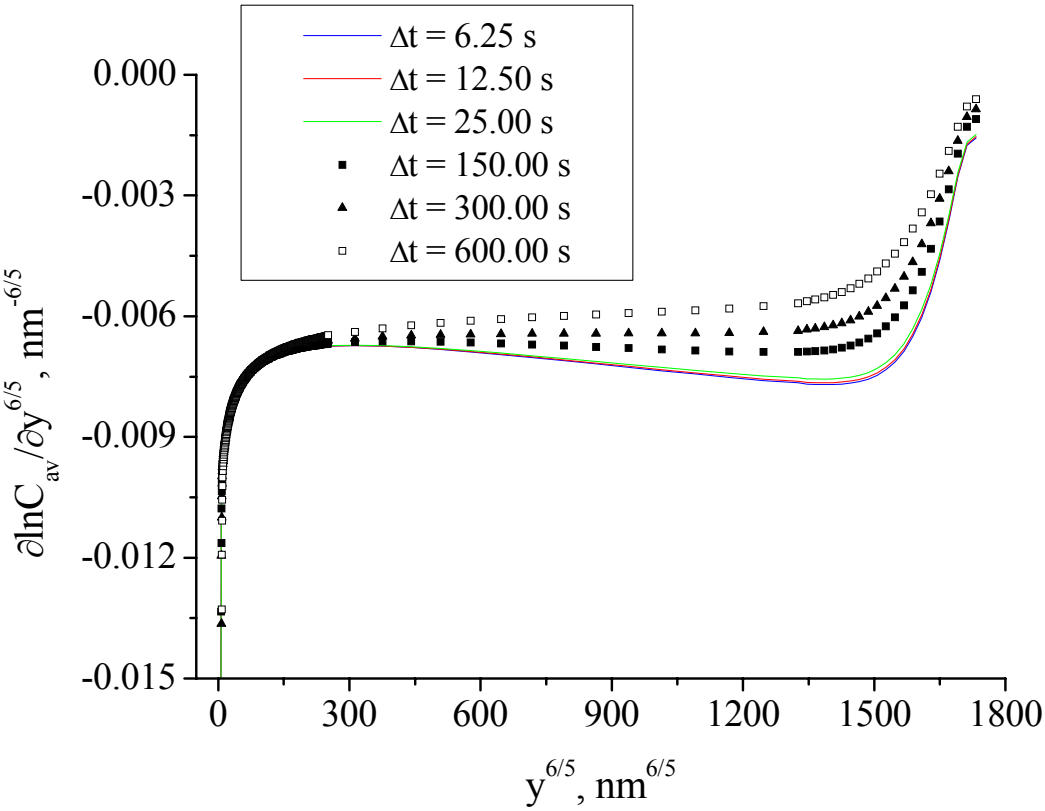

Fig. 4.5 A comparison of the derivatives of concentration profiles calculated by the FEM with different time intervals (Δt) at t = 2000 s.

account and analyzed. This is not true for a bicrystal, or an idealized system of parallel boundaries, because the profile is more nonlinear in this case according to Mishin. However, this opens the question about the validity of both methods (i.e., $\ln C_{av} = f(y^{6/5})$ and $\ln C_{av} = f(y)$) for polycrystals, what is also mentioned in [Kau95]. The other possible situations for L_{gb} being larger than d are discussed in the present work (fine-grained or ultrafine-grained materials [Mis95]). Nanocrystalline materials, characterized by grains of ten-hundreds of nanometers, have L_g of several or tens nanometers, what gives rise to β-values of the order of several thousands. The problems discussed above concerning the application of Le Claire's

relation (Eq. (1.16)) come into play together with the GBs orientations. The problems of GB orientations make the diffusion studies more complicated. In this sense the effects of small grain sizes are *size effects* – a term that arises particularly when discussing properties of nanocrystalline materials [Mai03], [Mai04a].

Two important points are taken into account now. First, the orientation of a GB to the surface is not analyzed. According to [Kau95], after the pre-diffusion anneals the GBs will tend to maximize the inclination angles with the surface in a way that most of their values will be around 90º. Moreover, the diffusion profile for real polycrystalline specimen represents an averaged resultant of the influence of different GBs orientations.

4.2.1 A comparison of the model of parallel boundaries with the model of square grains under conditions of type-B kinetics

The model of square grains used to analyze the corresponding diffusion effects represents a 2D pattern with GBs being simple lines perpendicular or parallel to the diffusion direction. Consequently, the concentration within the GBs is neglected. Each GB forms a side of square (fig. 4.6). Also the zero flux condition is used at the sample's bottom as a boundary condition. The typical grain sizes are 10, 25, 50 and 100 nm. Correspondingly, the grain size for the model of parallel boundaries simply means the distance between two neighboring GBs. The diffusion time was varied to cover different kinetic regimes, going from the B-regime to the A-regime. This allows one to apply different procedures used to deduce D_{gb}. The typical ratio of diffusivities Δ is $2.2 \cdot 10^4$, however in some cases smaller ratios are also used (it is indicated). Such ratios fit very well to all important requirements needed to be taken into account for the accuracy and convergence when simulating diffusion by FEM.

4.2.1.1 The model of parallel boundaries at short diffusion times

It is reasonable to start the analysis of the B-regime at short t with the model of parallel boundaries. Let us consider the variation of the distance between the boundaries from 10 nm to 100 nm. The diffusion process is analyzed at 2000 s. The values of diffusion parameters are the same as explained in chapter III. Under these conditions the contribution of GBs leads to the same slopes independently of d, whereas the bulk contribution (given by a complementary error-function) intermixed with the GB contribution changes. Because the average concentration (C_{av}) represents the grain concentration averaged along the direction

perpendicular to the GB, the GB part of the concentration is larger for smaller distances. This is confirmed by the result shown in fig. 4.8.

The GB part of the concentration reduces to a constant value when the distance is doubled (the results for d = 12.5, 25, 50 and 100 nm in fig. 4.7). Consequently, smaller deviations of the concentration C_{av} in the bulk part of the profile result for the larger distances. For larger d the bulk parts of the profiles are better determined by a complementary error-function solution (red curve in fig. 4.7). The strongest deviation appears, of course, for d = 10 nm, suggesting that this result will lead to serious errors in determining D_g from the corresponding profile. This is ascribed to an additional effect related to the small grain sizes. In order to emphasize the effect, the concentration profiles for the same parameters were calculated for the micrometer regime (fig. 4.7).

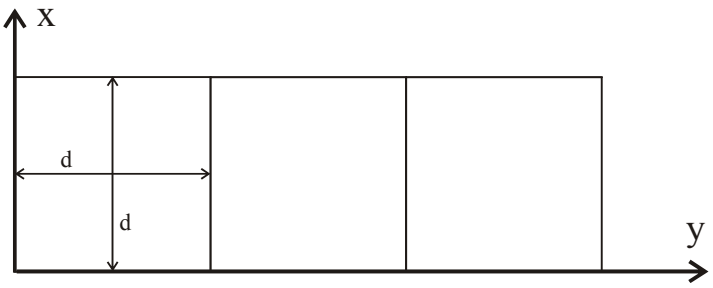

Fig. 4.6 Schematic representation of the square grain model.

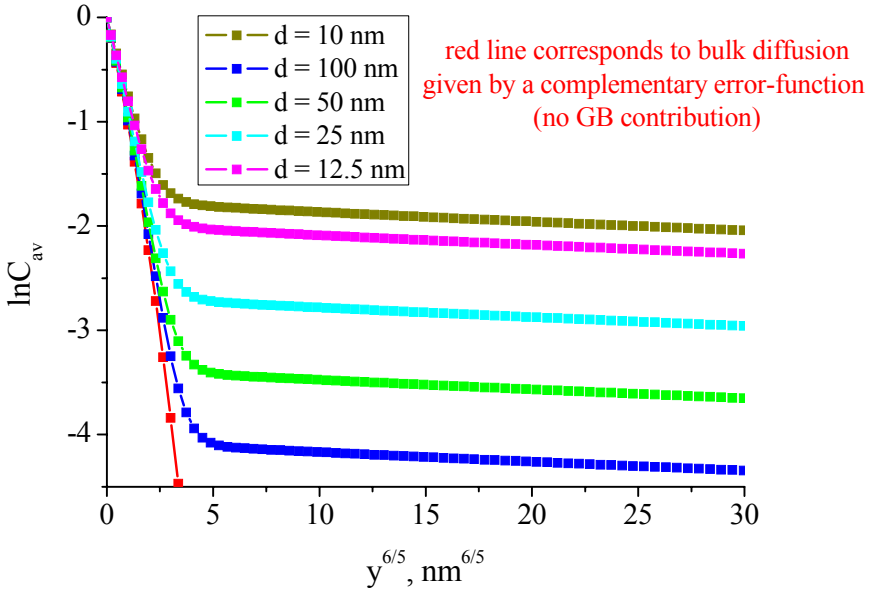

Fig. 4.7 Variation of $\ln C_{av}$ with $y^{6/5}$ calculated for the model of parallel boundaries for different distances between the boundaries (d).

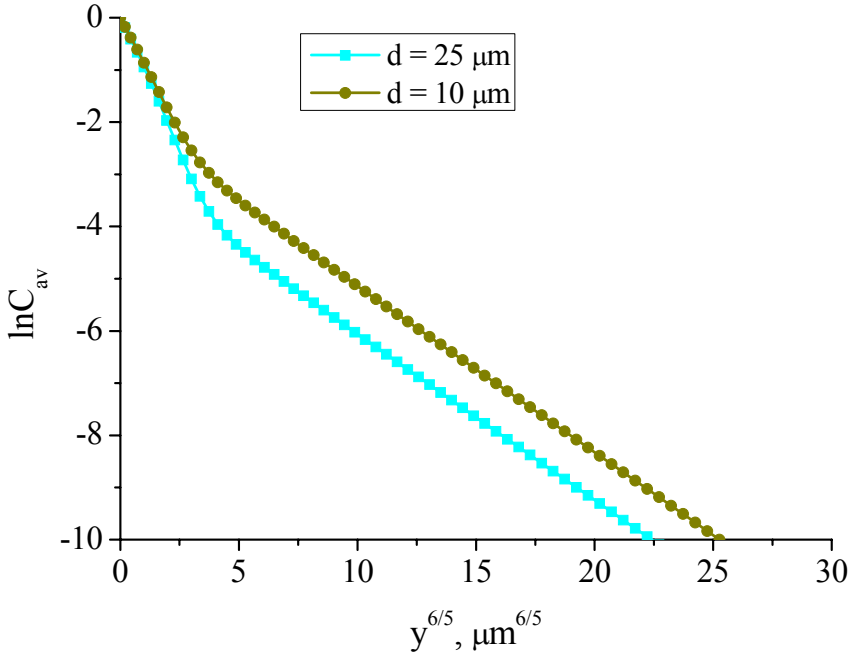

Fig. 4.8 Variation of $\ln C_{av}$ with $y^{6/5}$ calculated for $\Delta = 2.2 \cdot 10^4$ at $t = 2.04 \cdot 10^9$ s for the model of parallel boundaries.

The diffusion length in the grain (L_g) at $t = 2.04 \cdot 10^9$ s is about 0.78 μm for the profiles in fig. 4.8. This is exactly by three orders of magnitude higher than that at t = 2000 s. The deviations in the bulk parts for the profiles for different d are smaller in comparison with the nanometer regime. The GB part is affected in a way the two distinguishable parts of the profiles disappear with time (very small values of β arise). The profiles are less acute (between the two parts of the profiles) in fig. 4.8 in comparison with fig. 4.7. The slopes of the GB parts of the profiles shown in fig. 4.7 or in fig. 4.8 are the same for varying corresponding d. Clearly, the slope can then be changed only by varying t, if Δ is fixed. Yet, the profile in a nanoregime is more sensitive to the distance d. The process in the grain has not enough time to adopt a complementary error-function at very short t. In fig. 4.9 the diffusion profiles as shown in fig. 4.7 and fig. 4.8 for d = 25 and 10 nm and d = 25 and 10 μm are presented again together with the corresponding complementary error-function solutions to analyze the transition from the bulk diffusion parts to the GB parts of the profiles on different scales. The deviation of the result for d = 10 nm from its bulk diffusion profile is larger than that for d = 10 μm. Interestingly, the profiles in fig. 4.9b correspond mostly to bulk diffusion and only partly to the intermixture of the bulk and the GB parts, whereas on the nanoscale the GB part is very distinguishable despite the reduced values of y.

Understanding the diffusion process at different time scales allows one to analyze the role of GBs in the model of square grains or in one of the general representations of a polycrystal. The short times lead to an artificial prolongation of the process along GBs and, as a result, the GBs orientation can play a role. In these cases L_{gb} is typically much larger than d, and the kinetics are slightly different in comparison with the coarse-grained materials.

4.2.1.2 The model of square grains at short diffusion times

Let us *first* compare the profiles calculated for the square grains with the corresponding profiles for the parallel boundaries at fixed t. In fig. 4.10 the profiles are performed for these two models for $\Delta = 2.2 \cdot 10^4$ at t = 2000 s and for d = 25 nm and 100 nm. The profile for the square grains comprises two types of diffusion paths, namely parallel and perpendicular ones. The perpendicular GBs lead to spikes clearly seen in fig. 4.10. The number of these perpendicular paths is 19 for d = 25 nm and 4 for d = 100 nm for the fixed total length of the sample (geometry) of 500 nm. Each of them contributes to the profile changing the slope of it. It is seen that the discrepancy between the two models is more pronounced for smaller d. Moreover, one can recall here the effect of nonlinearity discussed in chapter III. When increasing the volume fraction of GBs (g) or decreasing d, the effect of nonlinearity is further induced, especially at very deep parts of the profiles (figs. 4.10b and 4.11).

When, *second*, analyzing the effect of g, one should be especially careful with the slope of the profile. The slope increases with decreasing d (fig. 4.11). The atoms move through the perpendicular and parallel boundaries in the model of square grains, and their concentration should be decreased in comparison with the motion of those along the parallel paths only. Surely, if the number of perpendicular GBs is higher, the concentration reduces. Consequently, two effects characterize the diffusion profile. One is related to increasing/decreasing d and leads to larger concentrations for smaller distances d, especially at coordinates close to the surface (fig. 4.11). Another one also depends on d and with decreasing d leads to smaller concentrations in comparison with the parallel boundaries. If the distance d is 25 or 10 nm, there is a convex curvature of the profile, because the perpendicular boundaries do not allow the number of atoms to be increased. This is in contrast to d = 50 or 100 nm, when the concentration increases at the deeper parts of the profile for the fixed length of the sample. If one believes that the model of square grains indeed represents a general polycrystal, then the GBs orientations can change the values of $D_{gb,app}$ applying Le Claire's

a)

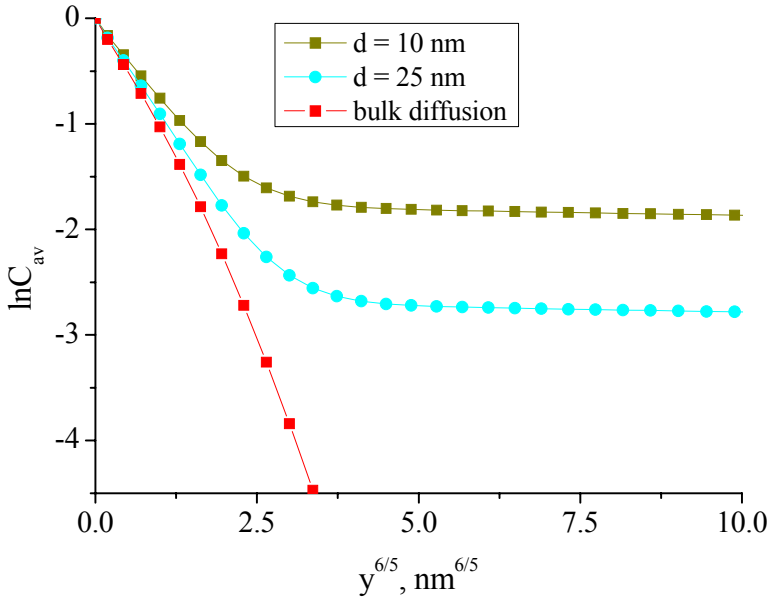

b)

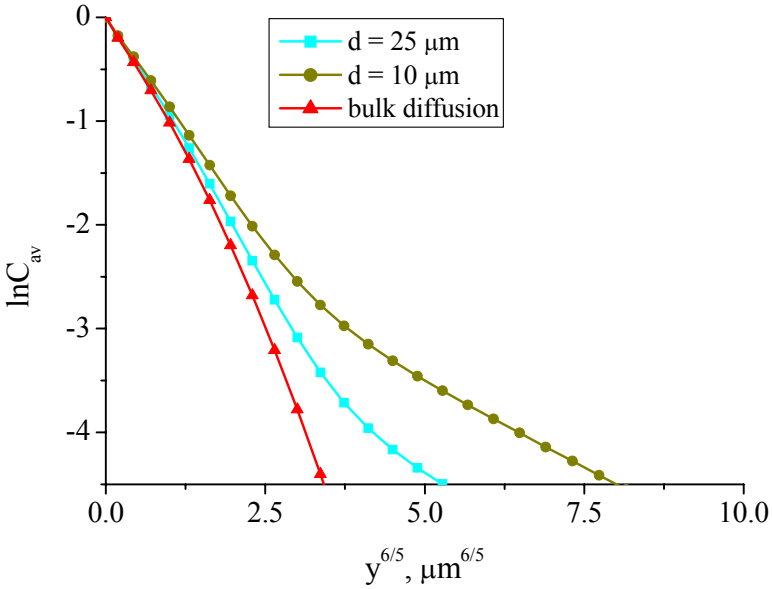

Fig. 4.9 A comparison of the diffusion profiles calculated at t = 2000 s a) and t = $2.04 \cdot 10^9$ s b) for different distances between the parallel boundaries (the same profiles as performed in figs. 4.7 and 4.8, but for another scale of $y^{6/5}$).

relation (Eq. (1.16)). The larger the slope the smaller the value of $D_{gb,app}$. Such an underestimation of D_{gb} is very typical for short t in the model of square grains in the type-B kinetics. The slope of the profile varies with t as well as with d. In order to estimate possible errors all the profiles presented in fig. 4.11 were fitted by straight lines. Accordingly, table 4.2 contains information on varying $D_{gb,app}$ determined by applying Le Claire's relation. Also the results of fitting the profiles calculated for the parallel boundaries are presented. As it is expected, all the slopes for the square grains are larger than for the parallel boundaries. It is important to notice that the slopes presented in table. 4.2 may only be compared with the slope of –0.00675, giving $D_{gb,app} = 4.22$ nm^2/s which itself is erroneous ($D_{gb,true} = 6.42$ nm^2/s). The latter value includes the corrected Le Claire's constant, but is affected by the effect of nonlinearity. Consequently, $D_{gb,app}$ can be three times smaller than the true value applying the conventional analysis when the effects of GBs orientations are not taken into account. The underestimation can be even larger, if the profile is measured (or calculated) for deeper coordinates influenced by larger number of perpendicular GBs.

Analyzing the derivatives of the profiles in the grain closest to the surface (fig. 4.12) reveals that the maximum is not reached even for d = 100 nm due to the perpendicular boundaries, since the position of maximum $y_{max}^{6/5} \approx 300$ nm$^{6/5}$ at t = 2000 s for $\Delta = 2.2 \cdot 10^4$. The positions of perpendicular GBs are 15.85, 47.59, 251.19 nm$^{6/5}$ for d = 10, 25, 100 nm, respectively. Moreover, the effect of perpendicular GBs is reflected in the increasing derivative in fig. 4.12. The peaks (spikes) in the diffusion profiles are broadened (red curve in fig. 4.12), i.e. their contribution can be characterized by certain widths.

Table 4.2 The slopes and values of $D_{gb,app}$ calculated by fitting the diffusion profiles by straight lines for different d. The values of $D_{gb,app}$ should be compared with the value of 4.22 nm^2/s.

d, nm	Square grains		Parallel boundaries	
	-slope	$D_{gb,app}$, nm^2/s	-slope	$D_{gb,app}$, nm^2/s
10	0.0113	1.79	0.00713	3.85
25	0.01095	1.88	0.00714	3.84
50	0.0101	2.15	0.00715	3.83
100	0.00892	2.65	0.00716	3.82

a)

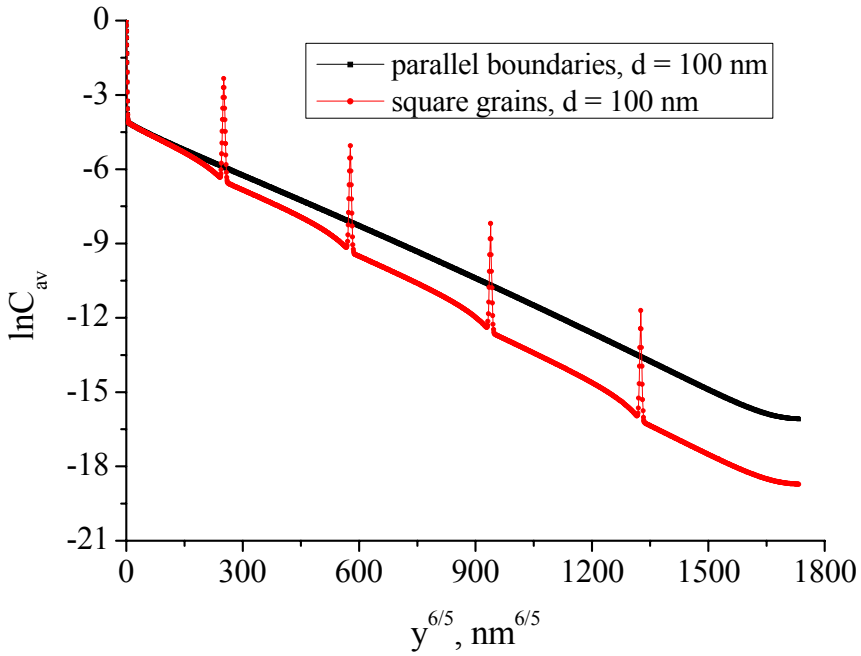

b)

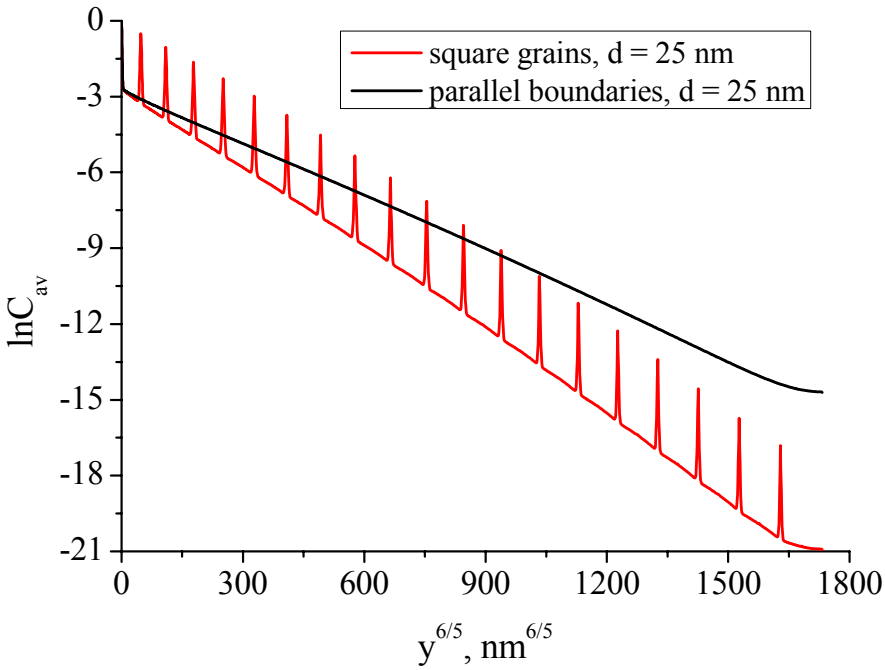

Fig. 4.10 Variation of $\ln C_{av}$ with $y^{6/5}$ calculated for two models with d = 100 nm a) and d = 25 nm b).

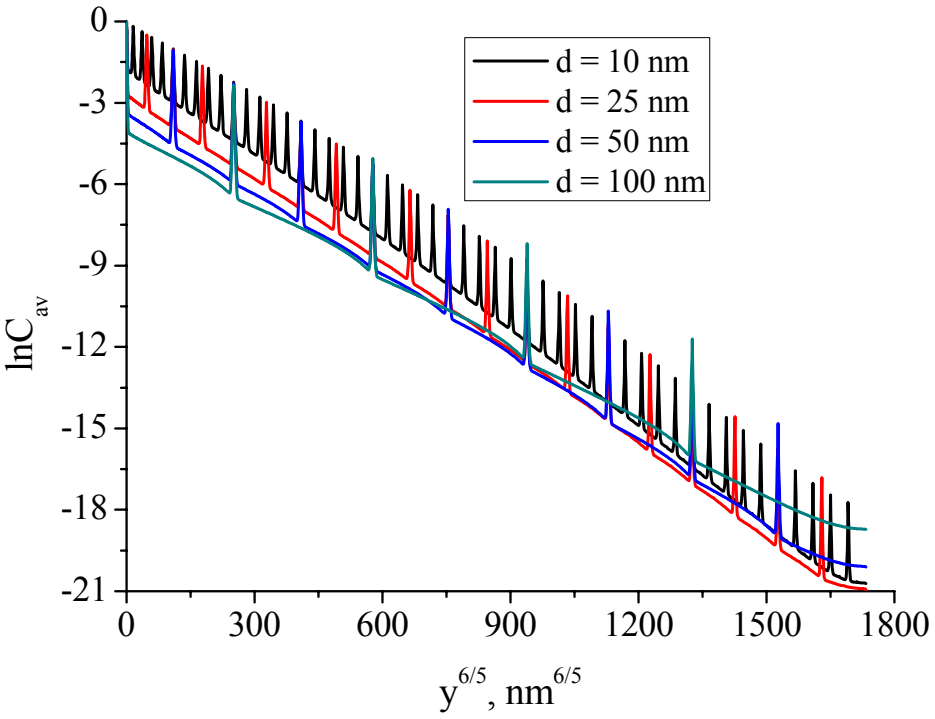

Fig. 4.11 A comparison of the diffusion profiles calculated for the model of square grains with different volume fractions of GBs.

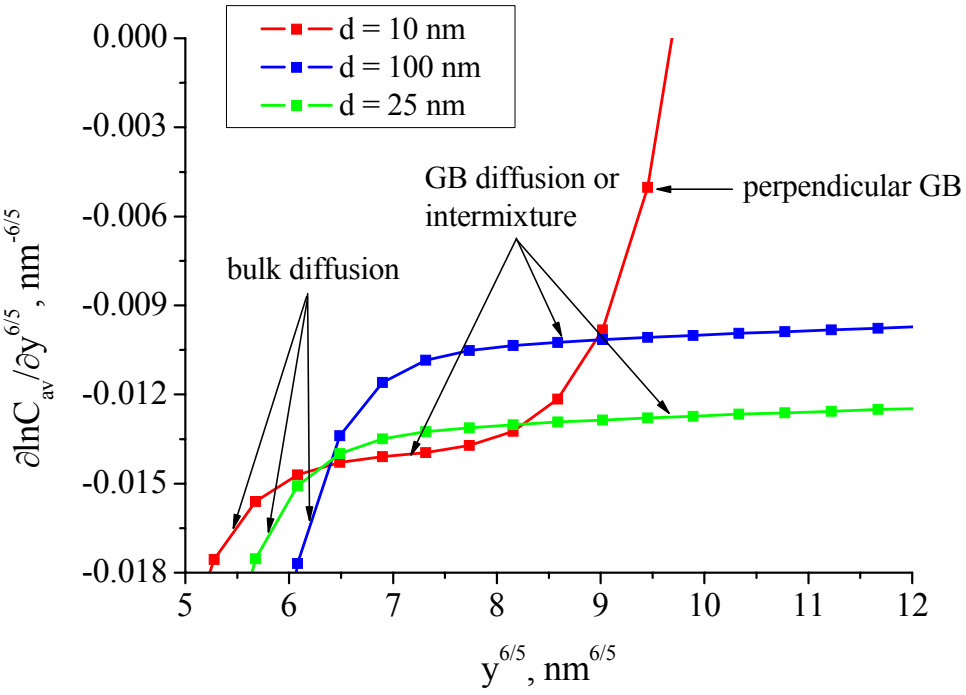

Fig. 4.12 A comparison of the derivatives $\partial \ln C_{av}/\partial y^{6/5}$ calculated for the model of square grains (only the first grain is taken into consideration) with d = 10, 25 and 100 nm.

A logical question arises when the model of square grains is used to simulate the diffusion profiles in a real microstructure, namely the question concerning different spatial orientation of GBs. The disadvantage of the model of square grains is that it comprises only perpendicular or parallel GBs. Can this model represent a realistic situation? In order to answer this question new models were proposed consisting of differently oriented GBs, i.e. GBs being not necessarily perpendicular to the diffusion direction. The models represent specific cases and may not exactly correspond to real polycrystals. However, the results obtained for these models give an important hint on the behavior of the diffusion process in realistic situations.

4.2.2 General geometrical models

4.2.2.1 Main characteristics of general geometrical models

Let us define the fist general model (denoted here as general geometry 1) comprising a unit with 17 GBs (6 parallel boundaries and 11 all others) of different orientations and lengths. The length (depth) of that unit is 250 nm, while the width is 40 nm. The unit was reflected once with respect to y = 250 nm for simulating diffusion at different time scales. Finally, the geometry used to simulate diffusion was 40 nm in width and 500 nm in depth. The unit is presented in fig. 4.13a, where also the length of all GBs are shown which vary from 20.6 to 70 nm (= the longest parallel boundary). All parallel boundaries in this geometry are situated at x = 0 only. In this way the half of the real grains was realized, because the number of triangle elements in the mesh used is already about 710000. When creating the mesh, some grains were divided into rectangular and triangular parts (see a snapshot in window in fig. 4.13a) in order to have a mesh of high quality. The former always gives a mesh of the high quality, while the latter suffices from sharp angles between the boundaries. One can estimate that d = 30.5 nm in this geometry by summing the lengths of all boundaries and dividing the sum by the number of boundaries (see discussion below). The lengths of GBs being closer to the surface are about 25 nm. Diffusion was simulated at rather short t, not exceeding 13200 s for $\Delta = 2.2 \cdot 10^4$, and the results obtained can be compared to a real polycrystal having d = 25 nm, or a little bit larger. The angles between the GBs and the diffusion direction vary from 14º to 78.7º in the general geometry 1 except for the parallel boundaries having 0º. Varying GBs lengths and angles in a wide range allows the general geometry 1 to be adapted to a quite generalized situation.

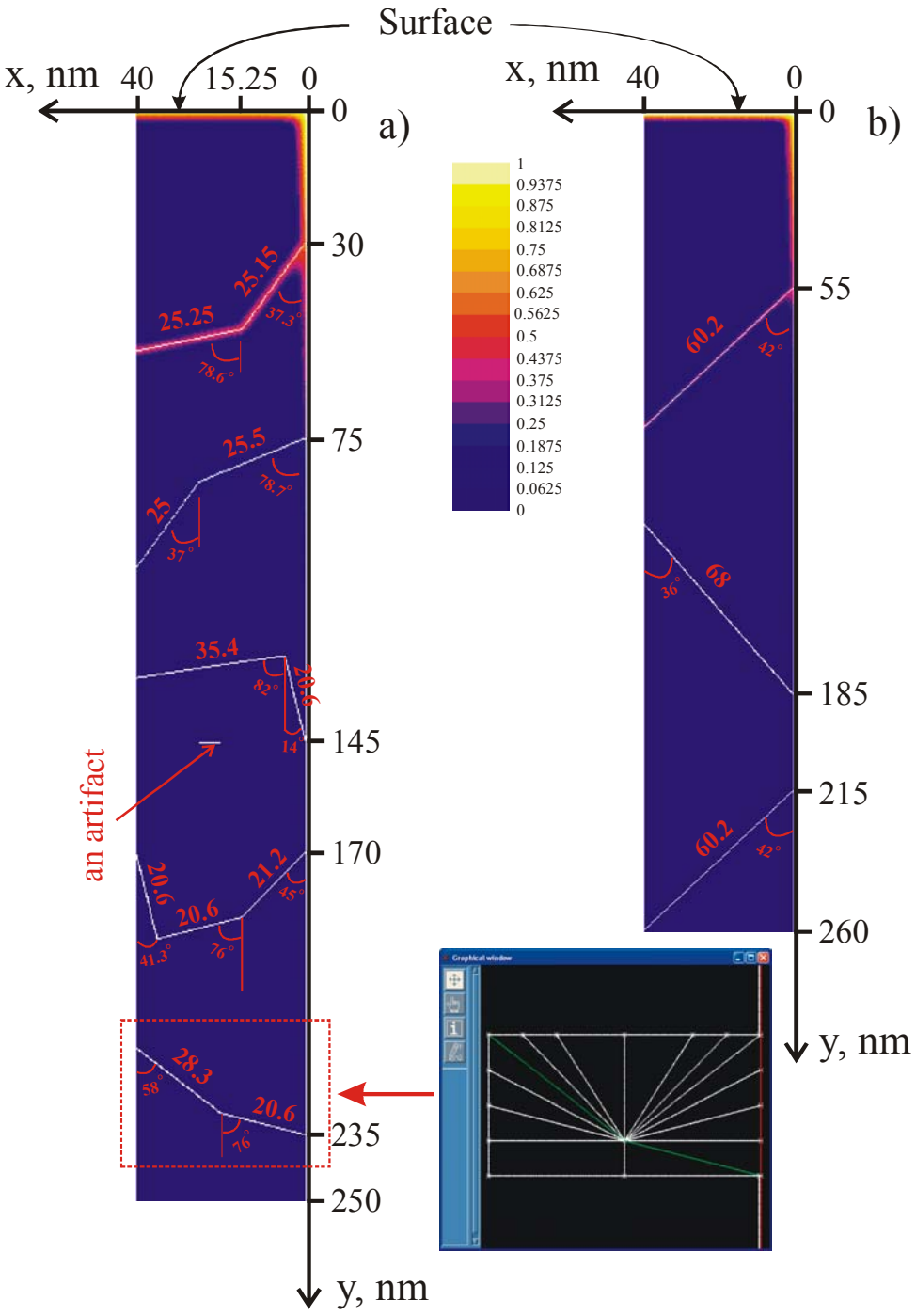

Fig. 4.13 Concentration distribution in the general geometry 1 (a) and general geometry 2 (b) at t = 8200 s for $\Delta = 2.2 \cdot 10^4$. The distribution is shown in colors, see explanation on the color pattern. White lines are GBs. In the window the fragment of the geometry drawn in the program SIMAIL [Sim95] is presented (red and green lines are GBs, white lines are additional lines used to make the quality of the mesh higher, i.e. the corresponding triangle and rectangular parts). Also the lengths of GBs in nm and their angles in degrees with respect to the diffusion direction are shown. An artifact means that in fact there is no GB at this place.

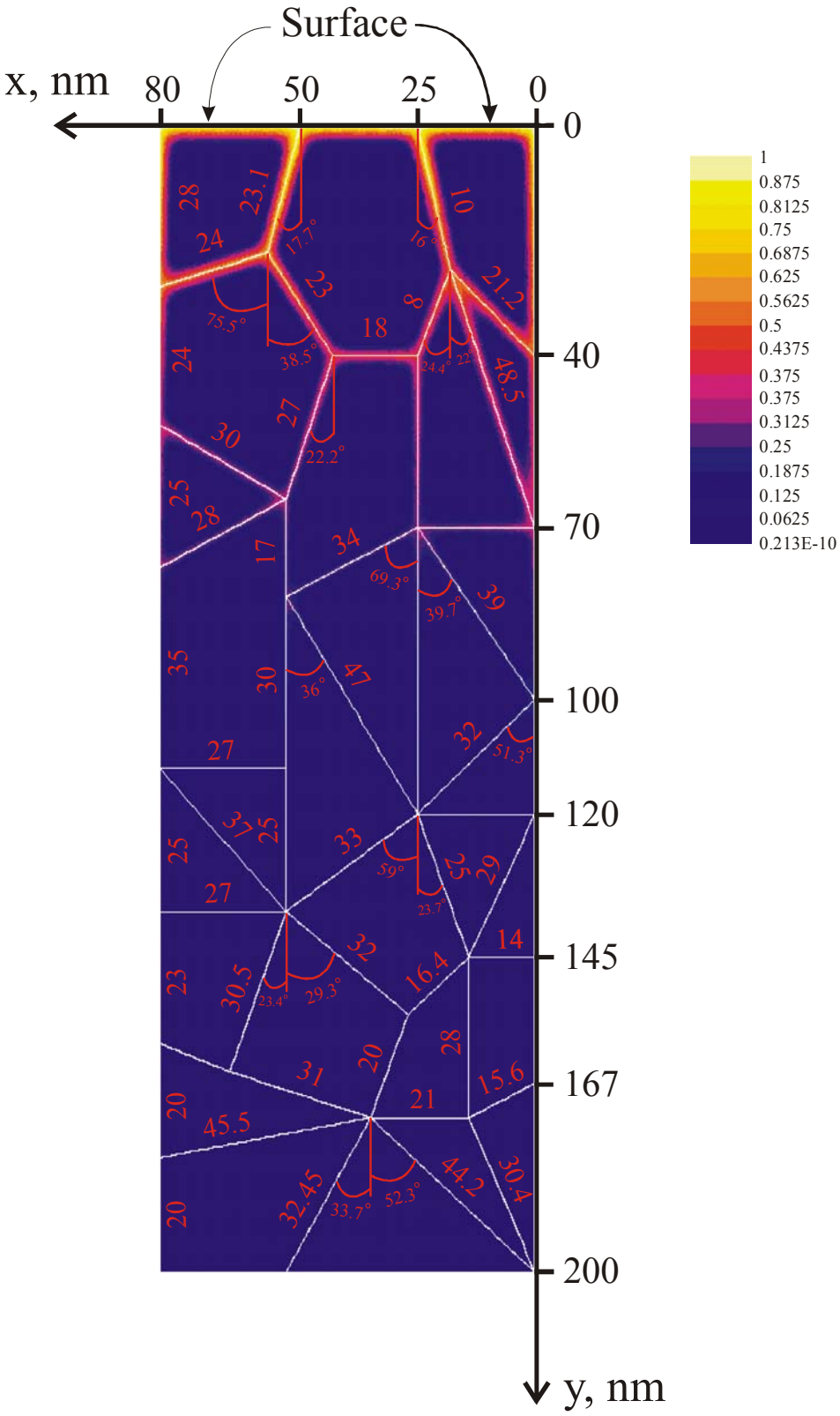

Fig. 4.14 Concentration distribution in the general geometry 3 at t = 8200 s for $\Delta = 2.2 \cdot 10^4$. The distribution is shown in colors, see explanation on the color pattern. White lines are GBs. The lengths of GBs are also shown. Only some angles with respect to the diffusion direction are indicated.

The general geometry 2 presented in fig. 4.13b is used for the same objective of analyzing the profile affected by different orientations of GBs. The unit is reflected at y = 260 nm. However, in this case d = 64 nm. The geometry is characterized by 4 parallel boundaries and 3 boundaries having the angles 42º and 36º to the diffusion direction.

One more general model (general geometry 3) was used with a larger number of grains and GBs in comparison with general geometries 1 and 2. The unit of this geometry is shown in fig. 4.14. The geometry consists of 57 GBs, including 21 parallel GBs. The lengths of GBs vary from 8 to 50 nm. The average grain size (d) was estimated to be 29.1 nm. So the results obtained for such a geometry should be comparable with those for d = 25 – 30 nm. As one can see, the geometry is twice as wide as for the general geometries 1 and 2. The problems of creating the mesh for this geometry become more serious than for the general geometries 1 and 2. Consequently, the number of triangle elements for this geometry is 355537 for the unit in fig. 4.14 and 710722 for the final geometry of the length 500 nm and of the width 160 nm. Using the general geometry 3, one should clarify the error introduced by the mesh of the smaller density. Advantage of this geometry is that the angles are very different, suggesting the contributions of very different boundaries. Additionally, some grains are very small, and these would be filled by diffusant in a very short t. This is a particular property of general geometry 3, which is important.

4.2.2.2 Simulation results obtained in the general geometrical models

All the geometrical models described so far were used to analyze the effects of GBs orientations. The lengths of the samples (geometrical models) were fixed to about 500 nm depending on the geometry, and the diffusion profiles were calculated at t = 8200 s for $\Delta = 2.2 \cdot 10^4$. The corresponding model of square grains exhibits 8 perpendicular GBs for d = 60 nm, if the GB at y = 540 nm (the length of the sample) is modeled as a reflecting boundary with the flux of atoms at this boundary being zero. As it was explained, the perpendicular boundaries lead to steeper diffusion profiles having spikes. That is why C_{av} was decreased in comparison with the model of parallel boundaries. However, the spikes themselves reflect increased concentrations around the perpendicular GBs. This effect is also confirmed in fig. 4.15, plotting the profile for square grains with d = 60 nm together with the profile calculated for the general geometry 2. The profile for the general geometry 2 has also the spikes slightly prolonged along the depth and, in principle; the profile is very close to that calculated for square grains. One GB in this model is oriented like having the angle with the parallel

boundary larger than 90º (the boundary of 68 nm in fig. 4.13b). It should be noted that the boundary gives a contribution to the profile with the angle 36º, because the concentration C_g is integrated along the x-direction varying y-coordinates from y = 0 nm to 520 nm. The difference of that boundary is reflected in the increasing concentration along the depth until its end is reached. The general geometry 1 has also several boundaries with the same effect. If the number of GBs is increased, this leads to further reduction of C_{av}, what increases the slope of the profile (black line in fig. 4.15, general geometry 1). Consequently, different slopes for general geometries 1 and 2 were observed despite the fixed t of 8200 s.

The profile calculated for the general geometry 1 could also be compared with that calculated for the square grains with d = 30 nm, because of similar grain size (d = 30.5 nm). The latter point is particularly important. As it is immediately seen in fig. 4.16, the profile for the general geometry 1 is characterized by the concentrations which are smaller than those for the square grains. This is related to the fact that the geometry under consideration has larger grain areas, which suggests reduced concentrations in the parts of the profiles close to the surface. Nevertheless, the slope of the profile for the general geometry 1 is slightly increased in comparison with the square grains of 30 nm. On the one hand, an increase of the slope is only possible, if the number of perpendicular GBs is larger. On the other hand, for the general geometry 1 the increase is related to the fact that the number of parallel boundaries in this geometry is smaller than the number of the others. The contribution of parallel boundaries exists but is not significant enough, i.e. mostly the other orientations affect the profile. Such situations are very difficult to predict, because the orientations can be different. Moreover, it is difficult to estimate d in such situations. Interestingly, d can also be estimated by taking the square root of the average grain area. According to this procedure, d was found to be about 40 nm for the general geometry 1. However, the larger grain size (in comparison with the square grains) would lead to a decrease of the slope.

Consequently, the slope of the concentration profile increases, if the number of parallel boundaries is smaller than all the others comparing these profiles with those for the square grains or when similar numbers of the two types of boundaries (parallel and perpendicular) comprise the geometry. Additionally, the profile for the general geometry 2 is not very much different from that for the square grains (fig. 4.15). In order to check this point further, the profile calculated for the general geometry 3 was analyzed, because this geometry comprises a large number of different GBs. In fig. 4.17 three profiles are compared, namely the profile for general geometry 1, the square grains with d = 25 nm and the general geometry 3. In the latter the number of GBs is by about a factor of 3 larger than in the general geometry

1. The number of parallel boundaries is extremely smaller than that of the others (there is no contribution of parallel diffusion paths at all). It is very significant, because the concentration once increased cannot be decreased sufficiently. This distinguishes the geometry from the general geometry 1. Additionally, some grains in the geometry are very small. These two facts cause some nonlinearity of the profile. Interestingly, the profile for the general geometry 3 is close to the profile for the model of square grains (both the profiles have d around 25 nm) and the slopes of those are believed to be similar. The decrease of the concentration at the coordinates close to the surface is similar in the two models. Because the model of square grains comprises the two extreme orientations, namely 0º and 90º with respect to the diffusion direction, it is supposed that the model of square grains is a good averaged representation of the real microcrystalline structure.

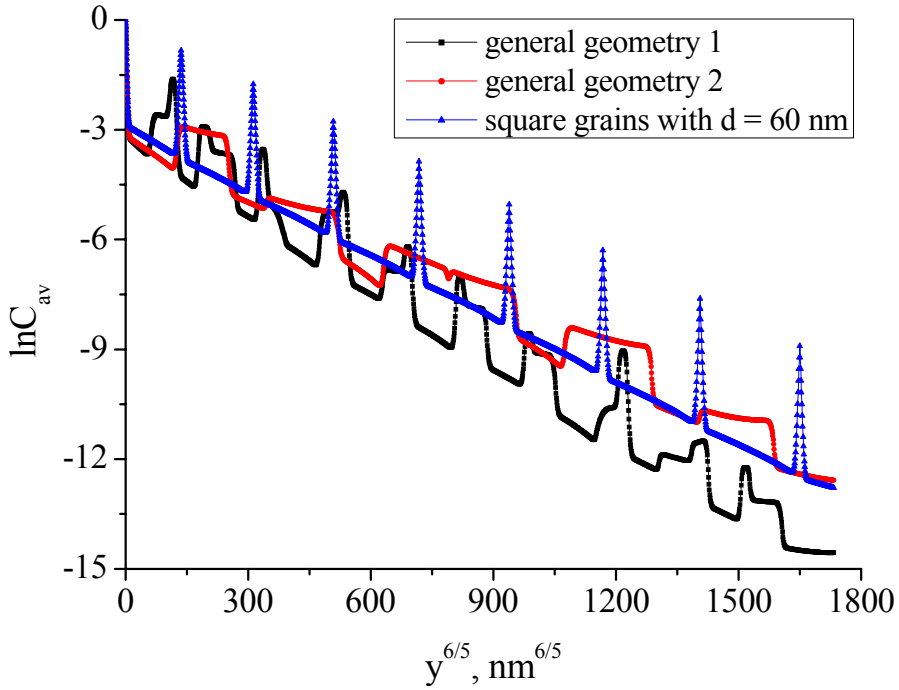

Fig. 4.15 A comparison of the diffusion profile of general geometry 2 with the profile of the model of square grains and general geometry 1. All the three profiles were calculated at t = 8200 s for $\Delta = 2.2 \cdot 10^4$.

The role of perpendicular boundaries is not the same at different t. It is, of course, related to the decreasing value of the parameter β (Eq. (1.9d)) with t. Thus, the parameter β yields information on the role of GBs orientations in the case of $L_{gb} >> d$. Of course, small values of β allow the contributions of perpendicular boundaries to be excluded (see discussion

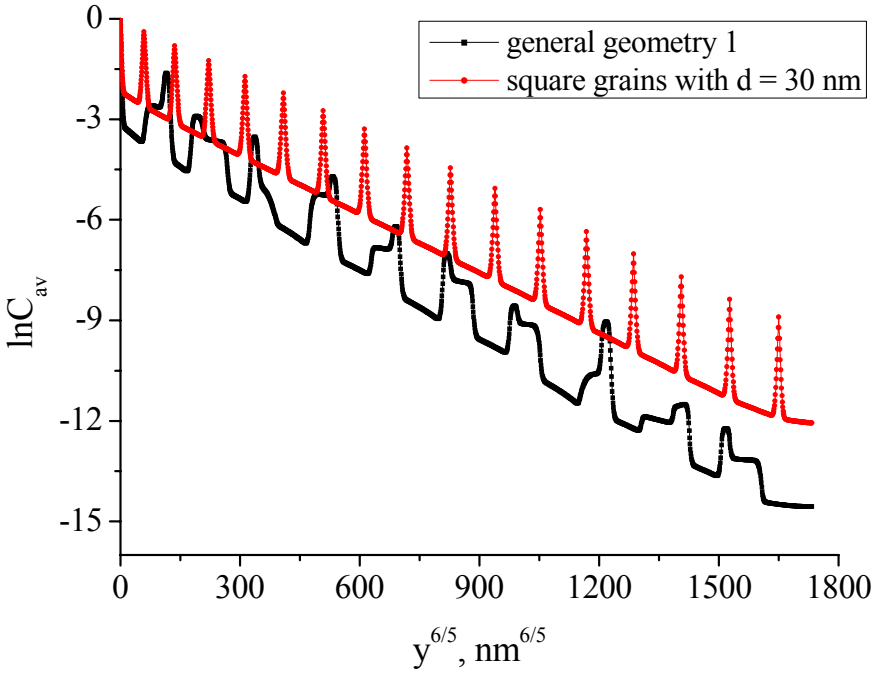

Fig. 4.16 A comparison of the diffusion profile of general geometry 1 with the profile of the model of square grains with d = 30 nm. All the profiles were calculated at t = 8200 s for $\Delta = 2.2 \cdot 10^4$.

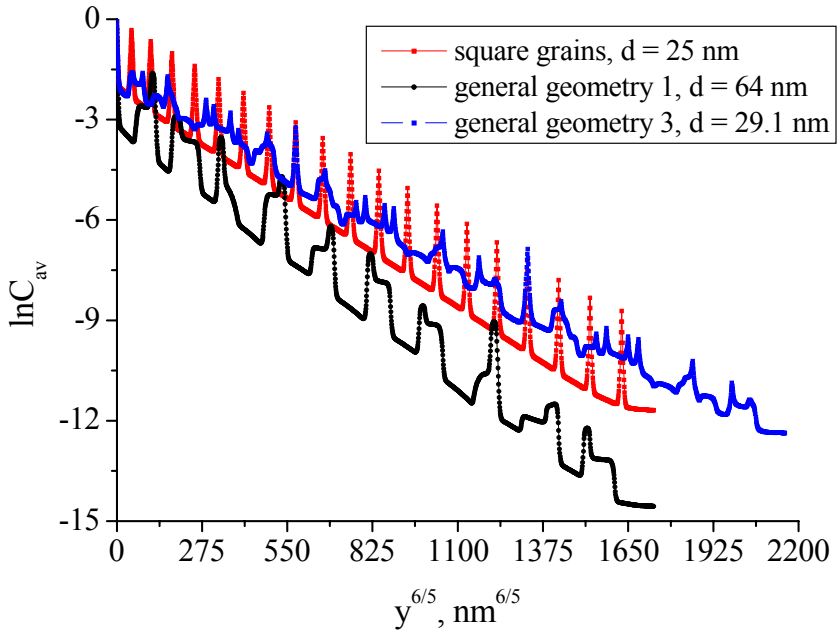

Fig. 4.17 A comparison of the diffusion profile of general geometry 3 with the profiles of the model of square grains with d = 25 nm and general geometry 1. All the three profiles were calculated at t = 8200 s for $\Delta = 2.2 \cdot 10^4$.

above). However, the A-regime starts when L_g is comparable with d, and in nanomaterials β remains high even when $L_g \approx d$. Nonetheless, the condition for starting the A-regime in nanomaterials is the same, and the contribution of perpendicular boundaries is negligible when $L_g \approx d$. This is confirmed by the result in fig. 4.18. The parameter β is around 182 at $t = 3 \cdot 10^6$ s and, for comparison, 3488 at t = 8200 s for $\Delta = 2.2 \cdot 10^4$. It is seen the two profiles for parallel boundaries and square grains coincide at long t. Below is given further analysis on the role of perpendicular boundaries.

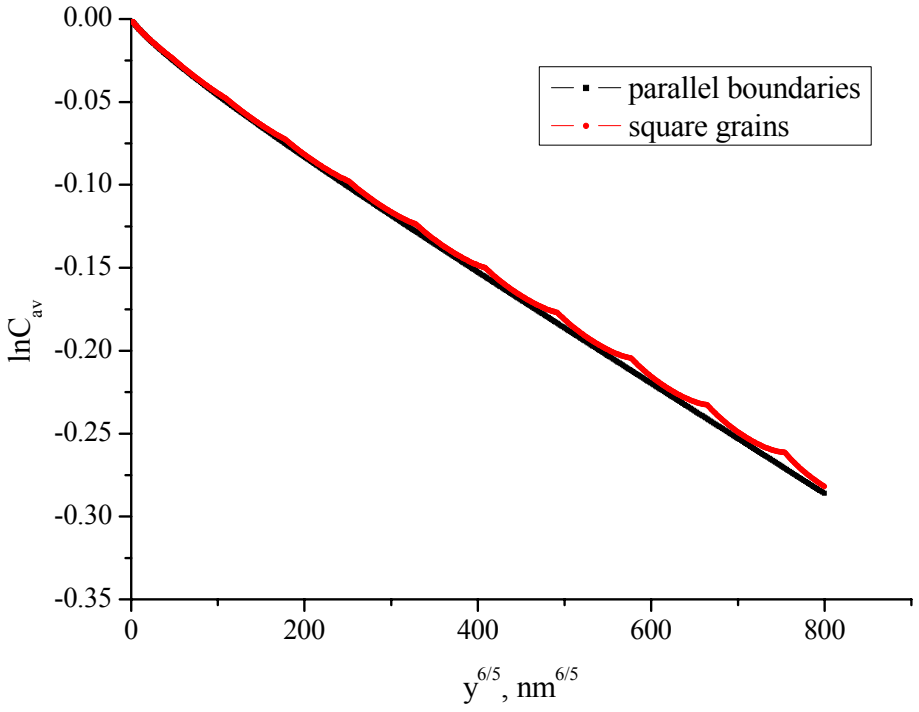

Fig. 4.18 A comparison of two profiles obtained for the model of square grains and the model of parallel boundaries at $t = 3 \cdot 10^6$ s for $\Delta = 2.2 \cdot 10^4$ (d = 25 nm, $L_g \approx 30$ nm). Parameters: β = 182, α = 0.17.

4.2.3 A comparison of the model of parallel boundaries with the model of square grains under conditions of type-A kinetics

As the model of square grains is a good representation of a realistic microstructure, the results for this model can be compared to those obtained for the model of parallel boundaries in the A-regime. Such a comparison would allow one to better understand the role of different evaluation equations in terms of extracting D_{gb} from the diffusion profiles measured in the A-regime. The A-regime is particularly important for nanocrystalline materials due to small grain sizes. One may simply define the A-regime to be observed, if L_g exceeds d (no matter to

which extent), while L_{gb} can be larger (nanomaterials) or smaller than d (coarse-grained materials). According to Monte-Carlo simulations of Belova and Murch [Bel01], the A-regime is observed when $d/\left(2L_g\right) \leq 0.4$. The role of GBs orientations is not sufficient in the A-regime due to the result in fig. 4.18. In order to better clarify this point the diffusion profiles were calculated for both the model of parallel boundaries and square grains at high t. The different equations (Eqs. (1.17)-(1.18)) were used in order to compare $D_{gb,app}$ with the true one. On the one hand, analysis of the equations has been started recently by Belova and Murch [Bel03], [Bel04]. Also a very interesting mathematical analysis was performed by Mishin [Mis92c] in order to suggest the expression for the effective diffusivity (D_{eff}) in heterogeneous media. On the other hand, the problem of D_{eff} has a very strong analogy with those problems dealing with conductivity in heterogeneous media which are discussed, for example, in [Lan78], [Gar95], [Harte04], [Kab05]. Most of these contributions concern Maxwell's (Maxwell-Garnett's) equation (Eq. (1.18)). However, Hart's equation (or Hart-Mortlock's equation for studying diffusion with segregation) is still remaining the only equation used for determining D_{gb} in the A-regime. Up to now one cannot find any experimental paper on D_{gb} measurement where Maxwell's or similar equation is used. It should also be noted, that Kalnin *et al.* [Kal02] modified Maxwell-Garnett's equation for the problems of segregation. Consequently, there is the purpose here to compare all these equations. Segregation is also studied varying the segregation coefficient (s) from very small to very large values. This implies the possibility to analyze D_{eff} under these different conditions, i.e. different values of s and geometries.

4.2.3.1 Analyzing the boundary condition at the bottom

The problem of the reflecting boundary becomes particularly important when simulating diffusion by FEM in the A-regime for a semi-infinite sample. However, for finite systems, for example, thin films, the reflecting boundary is a necessary condition [Gil76]. It is reasonable to analyze the boundary effect in order to estimate possible errors in determining D_{gb}. The increased diffusion lengths, especially L_{gb}, lead to the increase of concentration at the bottom of the sample and, thus, the concentration profiles affected by the reflecting boundary.

In fig. 4.19 the derivatives are performed for different lengths of the sample (the model of parallel boundaries) at $t = 7 \cdot 10^5$ s. The result corresponds to the B-regime, because

of $d/\left(2L_g\right) \approx 0.87$ at that time for $\Delta = 2.2 \cdot 10^4$. As one can see, the length of 500 nm may not be used for the analysis in the B-regime at so a high t, because the effect of the reflecting boundary becomes very strong – the maximum of the derivative is suppressed by this influence. The maximum appears, if the length is increased to 3200 nm. Interestingly, Shewmon [She63] explained that for an accurate experimental determination of the diffusivity (D) the concentration should decrease at least by an order of magnitude, what means a minimum penetration $y \approx 3\sqrt{Dt}$ (D is the diffusivity of a solute and t has its usual meaning). The diffusion length L_{gb} of 279.46 nm for $\Delta = 2.2 \cdot 10^4$ at $t = 7 \cdot 10^5$ s is only about twice as small as the length 500 nm. One needs to increase the length of the sample to guarantee several diffusion lengths and to calculate the diffusion profiles at appropriate times by using the FEM. The concentration profiles were also calculated in the A-regime for different lengths of the sample (fig. 4.20). It could be expected, that the boundary effect, arising in the B-regime, can alter the profile sufficiently in the A-regime too. For the length 1000 nm (fig. 4.20) C_{av} is about 0.70 at the bottom of the sample, while it is about zero at y = 3200 nm. Table 4.3 comprises the calculated diffusion lengths in the A-regime (L_{eff}) and the values of C_{av} at the bottom of the sample of different lengths for ratios Δ from 10^2 to 10^5 at $t = 5 \cdot 10^6$ s. The value of C_{av} at the bottom reflects the minimum concentration in the sample ($C_{av,min}$) except the point at the GB. The diffusion length L_{eff} was calculated according to $\sqrt{D_{eff}t}$, where D_{eff} was found by using Hart's equation (Eq. (1.17a)). The following three lengths of the sample are compared in table 4.3: 500 nm, 1000 nm and 3200 nm. Depending on the ratio Δ, the length can be chosen very long to exclude the boundary effect, keeping in mind the cost issue of computational time. In order to find the most suitable length for a particular case of $\Delta = 2.2 \cdot 10^4$, the values of $D_{gb,app}$ were calculated. According to table 4.3, the concentrations of about 0.90, 0.70 or even 0.30 (the corresponding $D_{gb,app}$ is not shown in the table) at the bottom may not be used, leading to significant errors. For instance, D_{gb} is overestimated by a factor of 26 for the length 1000 nm, because L_{eff} is larger than 1000 nm for $\Delta = 2.2 \cdot 10^4$ at $t = 5 \cdot 10^6$ s. The length of the model should be 3-4 times larger to obtain a reasonable result. If the ratio Δ is small ($= 10^2$), the length may be surely 500 nm to find D_{gb} accurately. The value of $C_{av,min}$ for $\Delta = 10^2$ and the length of 500 nm is so small, that D_{gb} is very accurate (not shown in the table), providing an error less than 1%. In a sense, this analysis confirmed suggestions of Shewmon for the experiment. If the profile is affected by the boundary in the B-regime, what is very possible with L_{gb} being only twice smaller that the length of the sample, $D_{gb,app}$ can be extremely large. In the present study, t was increased up to $50 \cdot 10^6$ s!

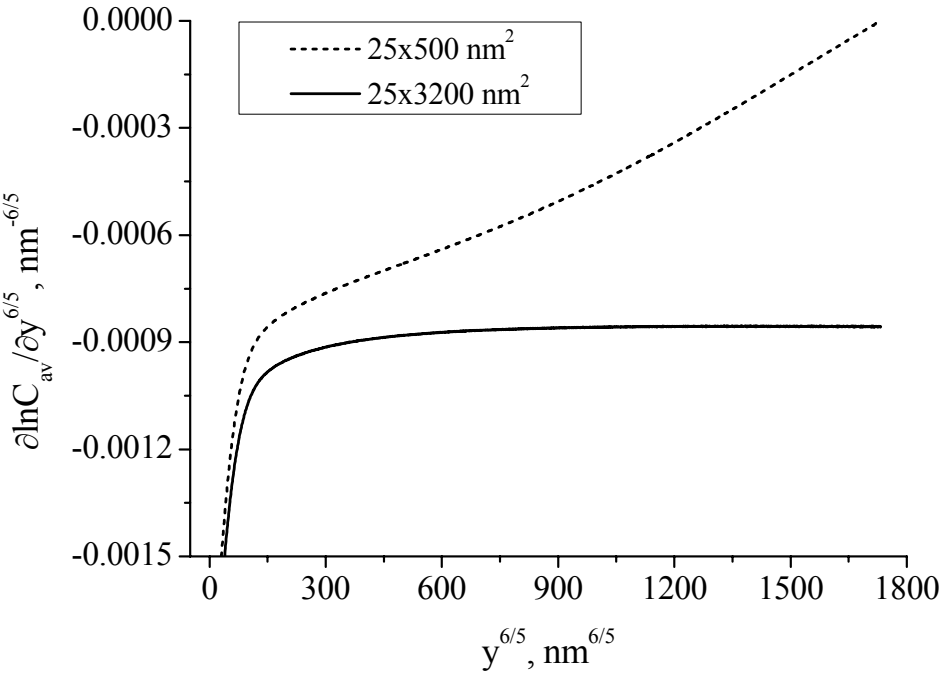

Fig. 4.19 Variation of the derivative $\partial \ln C_{av}/\partial y^{6/5}$ with $y^{6/5}$ calculated at $t = 7 \cdot 10^5$ s for $\Delta = 2.2 \cdot 10^4$ for the model of parallel boundaries of two lengths: a) 500 nm, b) 3200 nm.

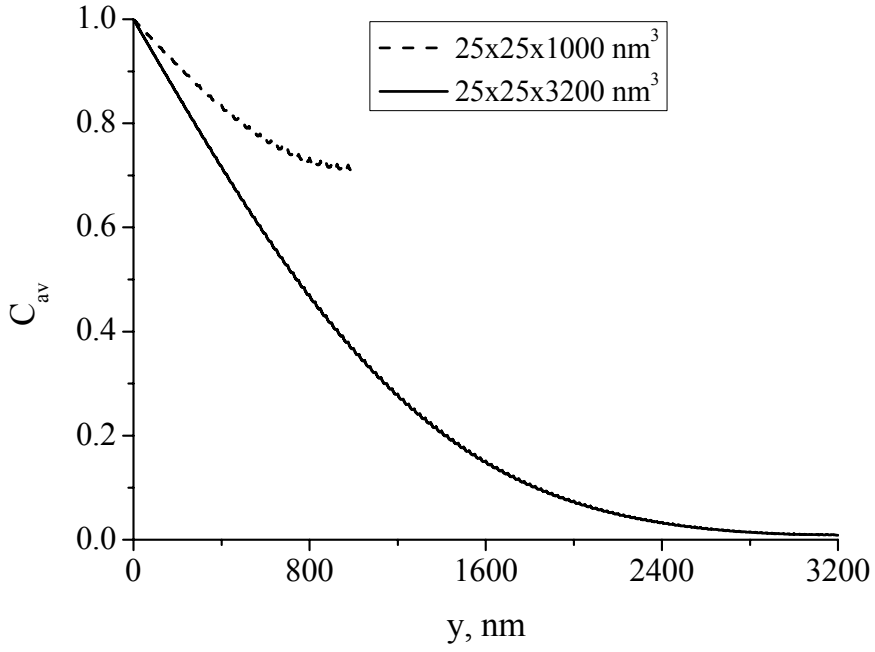

Fig. 4.20 Variation of C_{av} with y calculated at $t = 5 \cdot 10^6$ s for $\Delta = 2.2 \cdot 10^4$ for the model of square grains of two lengths: a) 1000 nm, b) 3200 nm.

For such high t much longer samples (geometries) are needed. Finally, the model of the length of 13000 nm was chosen as an appropriate one for different ratios Δ and t except $\Delta = 10^2$ for which the length was 1000 nm and 2000 nm for studying segregation effects (see discussion below).

Table 4.3 The minimum values of the average concentration ($C_{av,min}$) and diffusion lengths L_{eff} (Hart's equation, Eq. (1.17a)) calculated for different ratios of the diffusivities (Δ) and lengths of the sample (the model of square grains) at $t = 5 \cdot 10^6$ s. The average grain size (d) is assumed to be 25 nm. Also are presented the values of $D_{gb,app}$ calculated for $\Delta = 2.2 \cdot 10^4$ by using Hart's equation, i.e. these values should be compared with the true one of 6.42 nm^2/s*.

Δ	L_{eff}, nm	$C_{av,\,min}$			Type of material
		500 nm	1000 nm	3200 nm	
10^2	84	$4.68 \cdot 10^{-7}$	-	-	Coarse-grained
10^3	240	$8.05 \cdot 10^{-2}$	$1.81 \cdot 10^{-4}$	$2.45 \cdot 10^{-26}$	Fine-grained
$2.2 \cdot 10^4$	$1.11 \cdot 10^3$	$9.94 \cdot 10^{-1}$	$7.20 \cdot 10^{-1}$	$8.91 \cdot 10^{-3}$	Ultrafine-grained
10^5	2370	-	-	$3.47 \cdot 10^{-1}$	Ultrafine-grained
$D_{gb,app}$, nm^2/s		$2.26 \cdot 10^4$	$2.61 \cdot 10^1$	6.31	

*The values of $D_{gb,app}$ were calculated by using an improved procedure, see discussion below.

4.2.3.2 Analyzing Hart's equation and Maxwell-Garnett's equation

The A-regime is characterized by the fact that both the Hart equation and the Maxwell-Garnett equation suppose the steady-state condition of diffusion to be fulfilled. The area under the diffusion profiles calculated by FEM varies as t increases (fig. 4.21). This would imply slightly different diffusivities, found by Hart's or Maxwell's (Maxwell-Garnett) equation. As it will be shown below the latter discrepancy is insufficient. Moreover, as t is $50 \cdot 10^6$ s, the variation becomes extremely slow. In the present study the concentration profiles were calculated at very long t for the model of square grains and parallel boundaries leading to the conditions very close to the steady-state. The overall process is called here a quasi-steady-state diffusion.

The diffusion time was varied from $2 \cdot 10^6$ s to $50 \cdot 10^6$ s. However, the value of $50 \cdot 10^6$ s corresponds to 19 months and would unlikely be realized experimentally. Clearly, large absolute values of t are related to the temperature, since the diffusivities used in the simulation were quite small as being taken at 500ºC according to the Arrhenius dependences found in [Bro99a] for undoped ZrO_2. Increasing the temperature would allow one to decrease t. Anyway, as the A-regime is concerned one can think of the interacting GBs in the sense that

the atoms move between different boundaries, and one can apply the corresponding equations for D_{eff}.

Calculating the values of D_{eff} as a function of t for different Δ, different kinetic regimes were covered as proposed by Mishin [Mis95], namely the A- and A´-regimes. Since the GB and grain contributions are not separated in the A-regime, and the overall diffusion process is described by single diffusion equation with D_{eff}, the diffusivity D_{eff} was found by fitting the concentration profiles with a complementary error-function solution to diffusion equation using the program MATLAB. In this program a special toolbox was used for the fitting, namely the Optimization toolbox [Mat03], [Mat06]. The default values of optimization parameters of the standard function of the Optimization toolbox "lsqcurvefit" based on the nonlinear least-squares method [Ger03] were used for fitting. For instance, the total number of iterations was 400, whereas the absolute and relative errors were fixed to 10^{-6}.

The models of square grains and parallel boundaries are compared in fig. 4.22 for different Δ, t = $10 \cdot 10^6 - 50 \cdot 10^6$ s, fixed area fraction (2D geometry) of GBs (g) and fixed D_g. The larger ratio Δ yields increased values of D_{eff}. This can be understood by the fact, that D_{eff} is more determined by D_{gb} which is increased along the simulation for larger Δ. Moreover, increasing g (decreasing d) makes D_{eff} determined by D_{gb} only, as it is discussed in [Kau95]. In other words, the increase of D_{gb} leads to the same effects as the increase of g. The value of g was calculated as S_{gb}/S_{total}, where S_{gb} and S_{total} are the area given by GBs and the total area of 2D geometry (sample), respectively. Consequently, g for the model of square grains is twice as large as that for the model of parallel boundaries, if d is the same in both cases. For d = 25 nm g is about $1.96 \cdot 10^{-2}$ for the parallel boundaries and $3.84 \cdot 10^{-2}$ for the squares, if the length of the sample is 13000 nm. One has also to pay attention to the fact that D_{eff} is the same in the two models (fig. 4.22). It is related to the finding in fig. 4.18. According to these results, the role of perpendicular boundaries is negligible, if diffusion is studied in the type-A kinetics. Then it is interesting to compare the corresponding concentration distributions in order to clarify the latter point.

In fig. 4.23 a fragment of the concentration distribution in the model of parallel boundaries as well as in the model of square grains at t = $3 \cdot 10^6$ s for Δ = $2.2 \cdot 10^4$ is shown in color. The concentration variation from 0.6 to 0.3 corresponds to a depth range from 475 nm to 800 nm. Because the difference between the two models increases along the depth y (the diffusion regimes change with the depth), this range of the concentration was chosen as the most interesting one for the analysis of the role of perpendicular boundaries. The distributions for the two models completely coincide at higher concentrations. Similar values of

concentration were obtained in both models at the same depths. This confirms the idea about the negligibility of perpendicular GBs in the A-regime. The distributions are only slightly different at the points of the concentration level change. For instance, the concentration 0.375 arises at y ≈ 730 nm in the model of parallel boundaries, whereas it arises at y ≈ 755 nm in the model of square grains. What one is eventually interested in is the value of a calculated apparent GB diffusivity ($D_{gb,app}$).

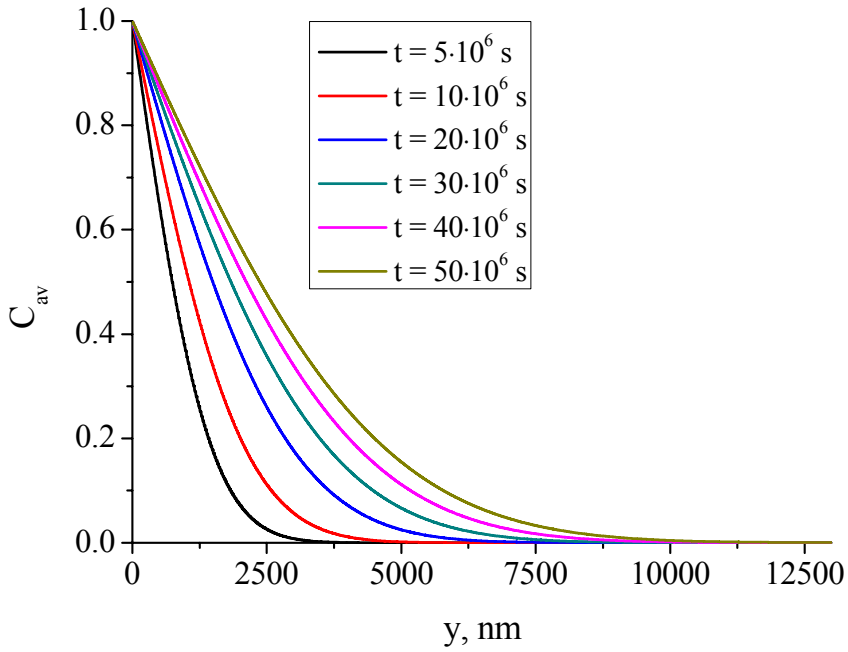

Fig. 4.21 Variation of C_{av} with y calculated at different t for $\Delta = 2.2 \cdot 10^4$ for the model of square grains.

Moreover, very recently Belova and Murch [Bel04] posed the question about the transition from the type-B kinetics to the type-A kinetics for the model of square grains. The answer to this question is given here due to the results in figs. 4.22 and 4.23: the condition for the transition in both the model of square grains and the model of parallel boundaries is the same (the condition $d/\left(2L_g\right) \leq 0.4$ was suggested by Belova and Murch for the model of parallel boundaries [Bel01]), since the role of perpendicular boundaries vanishes at high t. However, segregation of impurity atoms leads to another effect. In order to make a comparison of $D_{gb,app}$ with the true value, used in the simulation, for GB diffusion accompanied by segregation, two equations will be used: Hart's equation and Maxwell-Garnett's equation.

a)

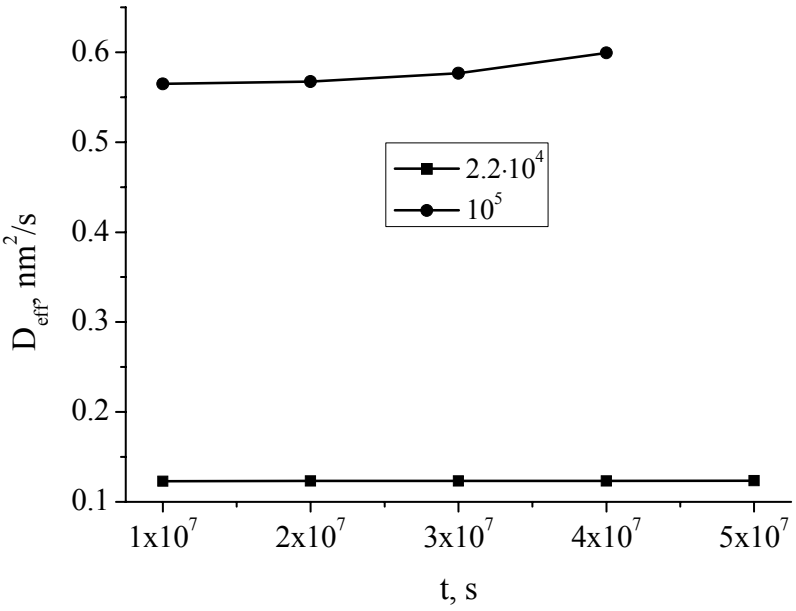

b)

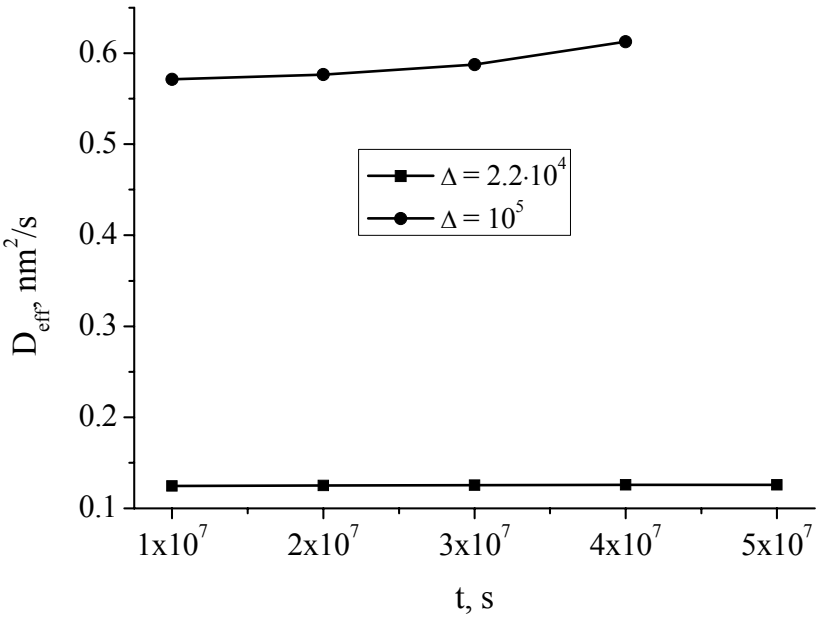

Fig. 4.22 Time evolution of D_{eff} for different ratios Δ: a) square grains, b) parallel boundaries.

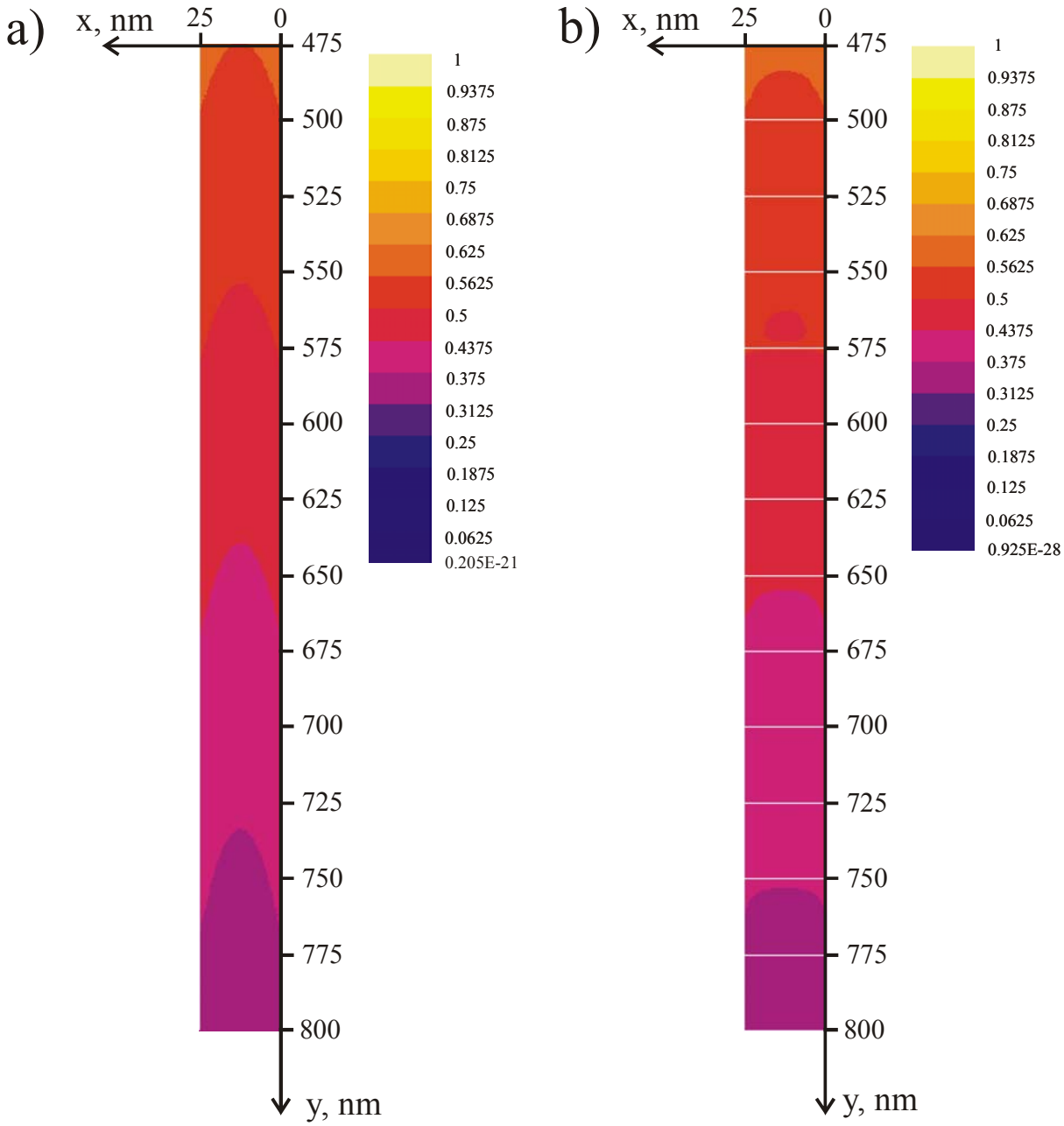

Fig. 4.23 A fragment of the concentration distribution at $t = 3 \cdot 10^6$ s: a) parallel boundaries, b) square grains. White lines represent to the perpendicular GBs with respect to the diffusion direction. The parallel boundaries in both distributions are at x = 0.0 and 25.0 nm. The corresponding color pattern is also shown.

4.2.3.3 Segregation effects under conditions of type-A kinetics

The Hart equation and its extended version for diffusion of impurities, known as Hart-Mortock's equation (Eq. (1.17b)), is widely used to deduce D_{gb}, if the diffusion profile is measured under conditions of the kinetics of type-A. As Belova and Murch [Bel03] showed, the Hart-Mortlock equation leads to errors of deducing D_{gb}, when simulating diffusion in the model of square grains varying g and fixing the segregation factor (s). In the present work another important point is addressed, namely the influence of segregation. Very often s is obtained by measuring the triple product $s\delta D_{gb}$ in the B-regime, if D_{gb} is known from the measurements in the C-regime [Her03]. However, the measurements in the C-regime are not always possible. Then one could combine the measurements in the B- and A-regime. When knowing the product sD_{gb} from the measurements in the B-regime, the only unknown parameter in the Hart-Mortlock equation or the Maxwell-Garnett equation is s. Can the Hart-Mortlock equation provide reasonable values for s? It is supposed that s can be used as the ratio of the corresponding concentrations in the GB and in the grain (Eq. (1.6b), very dilute conditions). The question of the validity of Hart-Mortlock's equation with respect to segregation has not been analyzed yet. Contrary, the Maxwell-Garnett equation was recently analyzed theoretically, extended to the problems of segregation and chemical diffusion [Kal02], [Jam06]. In the study of Belova and Murch [Bel03], it was proved that the Maxwell-Garnett equation gives smaller errors than Hart-Mortlock's equation varying g. Nevertheless, segregation imposes new conditions, i.e. suppresses the type-B kinetics. This is why it can be particularly interesting to analyze the equations under the conditions induced by the segregation.

Diffusion profiles were simulated in the model of parallel boundaries and in the model of square grains by using the modified Fisher system (Eq. (1.6c)). The average grain size (d) used in the simulation was fixed to 10 nm, whereas s was varied from 5 to 640. The value of s = 640 can be considered as a kind of maximum, because a further increase of s did not give a significant difference. However, larger values of s are also possible in different materials depending on temperature [Div01]. In fig. 4.24 the diffusion profiles calculated for varying s are depicted for fixed ratio $\Delta = 10^2$ and time $t = 10^6$ s. The length of the sample (geometry) was fixed to 2000 nm. The following property is reflected in fig. 4.24, the diffusion process with segregation is a nonlinear process going to some saturation, but never reaches it. In this sense, the situation is similar to the variation of t (fig. 4.21), i.e. the area under the curves varies with s.

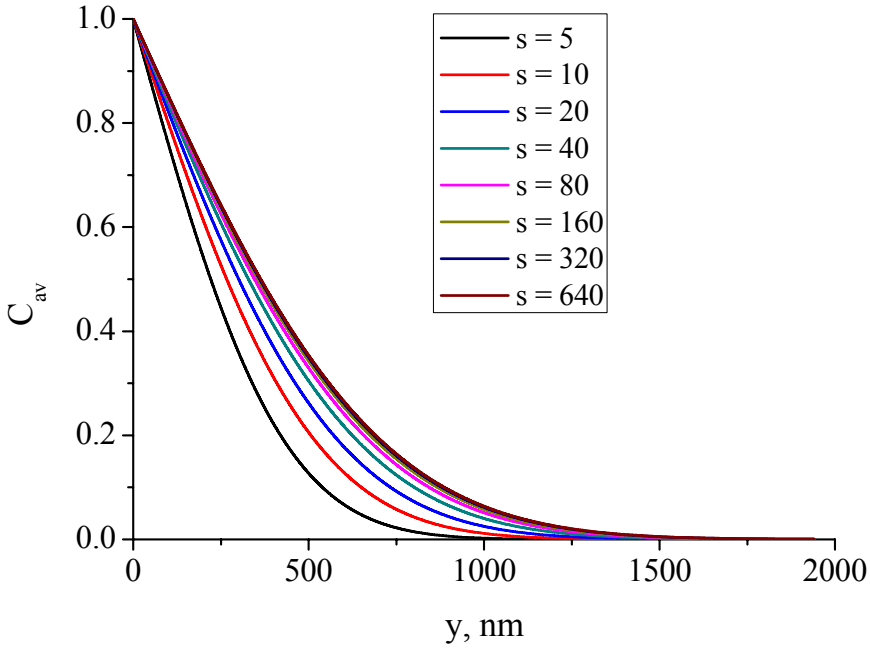

Fig. 4.24 Variation of C_{av} with y calculated for different segregation coefficients (s) for the model of square grains. The average grain size is 10 nm and $t = 10^6$ s.

Importantly, segregation suppresses the B-regime (Eqs. (1.10)-(1.11)) and gives larger values of L_{gb} (Eq. (1.12a)). Although, the rates of diffusion in the bulk are the same as in the case of diffusion without segregation. Segregation leads to larger values of β (Eq. (1.12b)) at the moment when the A-regime comes into play. This situation is similar to that for decreasing d. In both cases β can be very large even if $L_g \geq d$. It can be understood by the fact that segregation leads to an enhanced concentration within the GBs, because it restricts the contribution of GBs into the bulk (grain).

Following the procedure discussed in the preceding section, the diffusion profiles were fitted by a complementary error-function with the resulting D_{eff} being valid for a constant surface source as used in the simulation. Along with the fitting, the values of D_{eff} were estimated by using Hart-Mortlock's equation and Maxwell-Garnett's equation for each value of s. In fig. 4.25 the results of fitting are compared with those calculated by using the Hart-Mortlock and Maxwell-Garnett equations for the model of parallel boundaries as well as for the model of square grains. One can see the discrepancy that exists between the Hart-Mortlock equation and the simulation. The discrepancy increases with s, because the dependence of D_{eff} on s is linear in one case and nonlinear in another one. Contrary, Maxwell-Garnett's equation gives much more reasonable values for D_{eff}. This suggests that the linear

dependence supposed by the Hart-Mortlock equation is not valid even for the model of parallel boundaries when the Hart type equations are expected to be valid similarly to mixture rules [Nie78]. In fig. 4.26 the Maxwell-Garnett equation is compared separately with the simulation result. Interestingly, the deviation of Maxwell-Garnett's equation from the simulation is larger for the model of parallel boundaries. To estimate these deviations $D_{gb,app}$ was calculated by fitting the diffusion profiles by the complementary error-function with the Hart-Mortlock or Maxwell-Garnett type equations instead of a single D_{eff}, i.e. the fitting with respect to D_{gb} was done because all other parameters in the equations are known. The errors of determining D_{gb} were found from the fitting results and are summarized in table 4.4. The values of $D_{gb,app}$ are typically smaller than the true one ($D_{gb,true} = 2.95 \cdot 10^{-2}$ nm^2/s or $2.95 \cdot 10^{-14}$ mm^2/s). Moreover, the errors vary with s in most cases. Very large errors were observed by using the Hart-Mortlock equation for the model of square grains, and smaller errors of applying this equation to the model of parallel boundaries were found for s = 5-20. However, the error increases up to ~100% for both the models applying the Hart-Mortlock equation, if s = 640. The Maxwell-Garnett type equation gives very small errors for the model of square grains. An error of 5% observed when this equation is applied to the model of square grains can have a numerical origin. Nevertheless, an error of 95% was observed for the model of parallel boundaries when using the Maxwell-Garnett type equation. Moreover, the Maxwell-Garnett type equation overestimates D_{gb} by a factor of 2, if applied to the model of parallel boundaries. By putting into Maxwell-Garnett's equation the value of g corresponding to the square grains and applying it again to the model of parallel boundaries, the error (improved $D_{gb,app}$ and error in table 4.4) was decreased to about 58% for s = 40. This was done according to the finding in the present work, that the diffusion profiles calculated for the model of parallel boundaries and the model of square grains are very similar at high t, i.e. in the A-regime in the case of self-diffusion (figs. 4.18 and 4.22). The decrease of the error indicates that the use of this equation requires g to be calculated for the model of square grains even if applied to the model of parallel boundaries. Similarly, the Hart type equation is supposed to be valid for the model of square grains if g is calculated as for the model of parallel boundaries. But this is valid only with s = 1. Segregation implies that the coincidence of the diffusion profiles for s = 1 does not longer exist in the case of s > 1. Accordingly, a significant error still remained for larger s even after using an appropriate g applying Maxwell-Garnett equation to the model of parallel boundaries. Additionally, there is a possible saturation of D_{eff} as a function of s. Therefore, at very large s the s-variation is close to steady-state with respect to that parameter.

a)

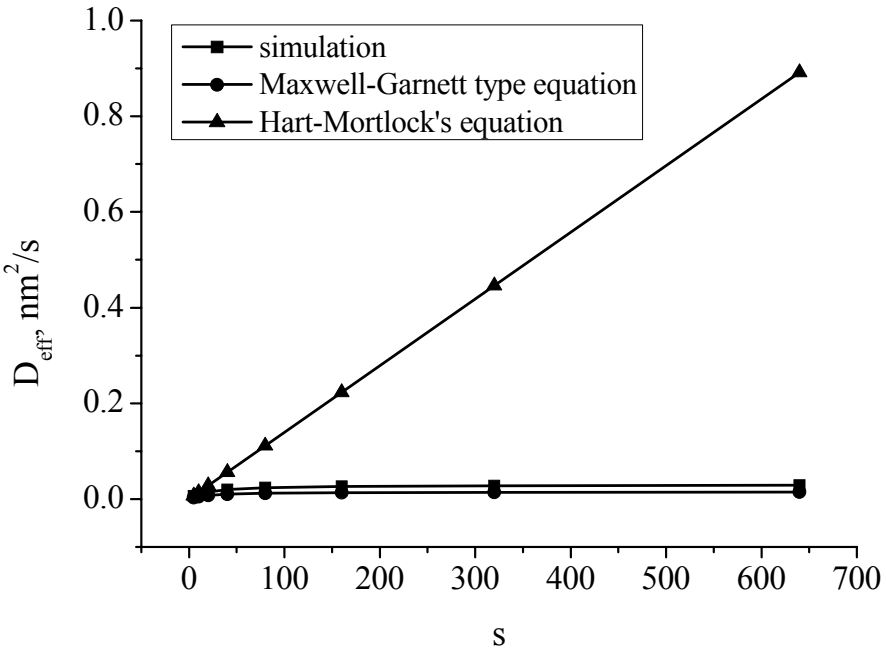

b)

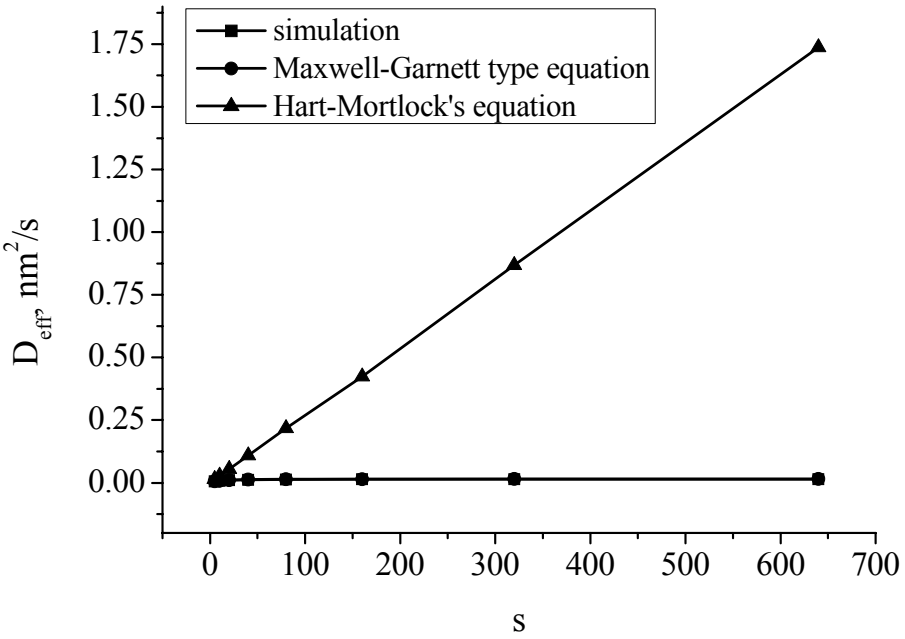

Fig. 4.25 Effective diffusivities obtained by fitting the simulated diffusion profiles to a complementary error-function for the model of parallel boundaries a) and the model of square grains b).

a)

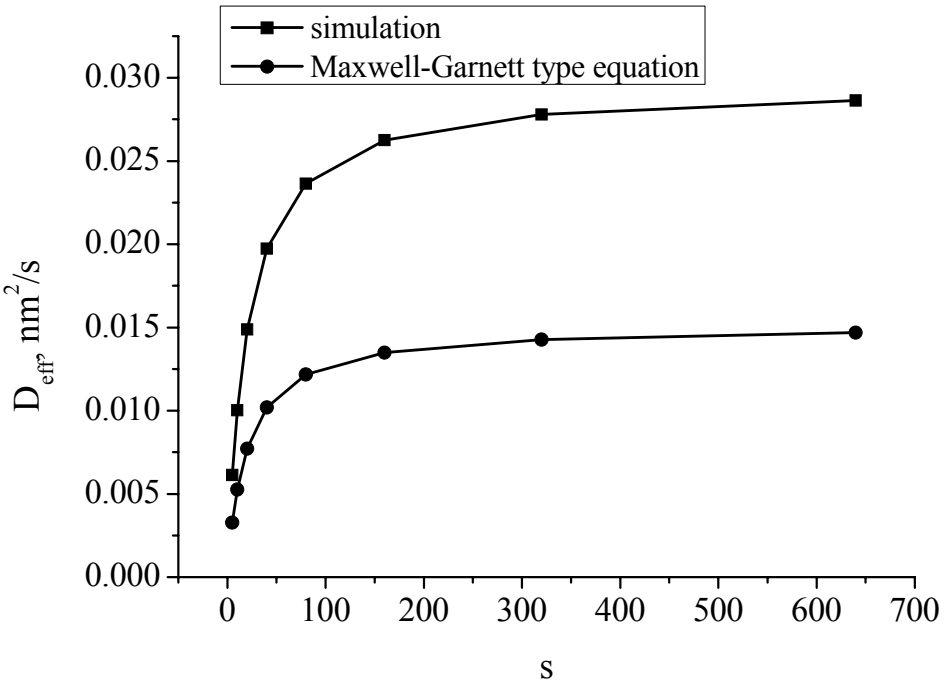

b)

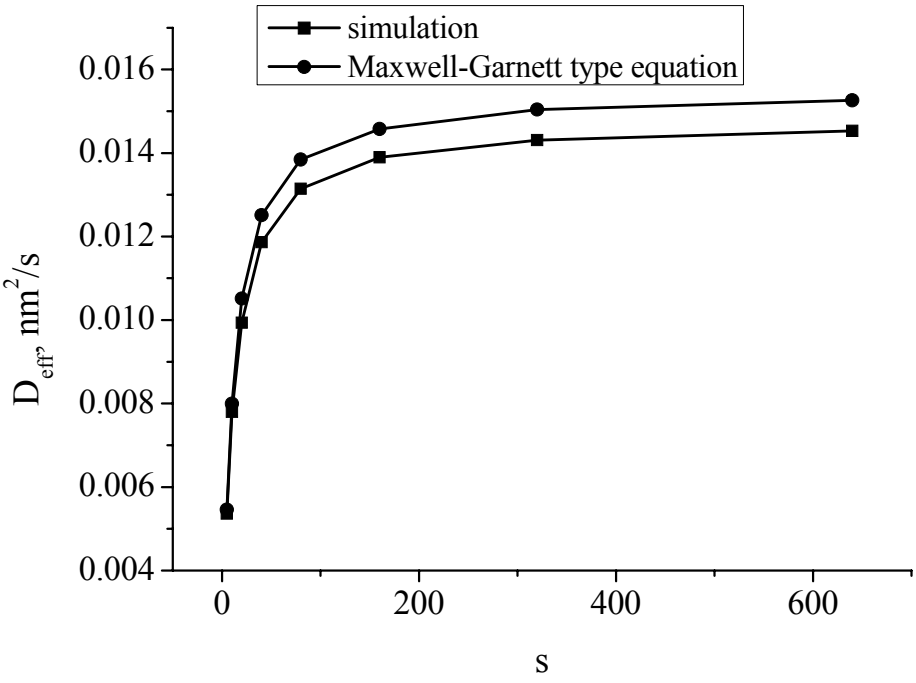

Fig. 4.26 A comparison of the simulation results with the Maxwell-Garnett type equation for the model of parallel boundaries a) and square grains b).

Table 4.4 The values of $D_{gb,app}$ and the errors of finding D_{gb} found from the simulated diffusion profiles by using the Maxwell-Garnett equation and the Hart-Mortlock equation for the model of parallel boundaries a) and the model of square grains b). $D_{gb,true} = 2.95 \cdot 10^{-2}$ nm^2/s.

a)

s	$D_{gb,app}$ due to Hart-Mortlock's eq., nm^2/s	Error in % due to Hart-Mortlock's eq.	$D_{gb,app}$ due to Maxwell-Garnett's eq., nm^2/s	Error in % due to Maxwell-Garnett's eq.	Improved $D_{gb,app}$ due to Maxwell-Garnett's eq., nm^2/s	Error in % due to improved Maxwell-Garnett's eq.
5	$2.48 \cdot 10^{-2}$	16	$5.74 \cdot 10^{-2}$	94	$3.33 \cdot 10^{-2}$	13
10	$2.07 \cdot 10^{-2}$	30	$5.75 \cdot 10^{-2}$	94	$3.72 \cdot 10^{-2}$	26
20	$1.56 \cdot 10^{-2}$	47	$5.75 \cdot 10^{-2}$	94	$4.20 \cdot 10^{-2}$	42
40	$1.05 \cdot 10^{-2}$	64	$5.75 \cdot 10^{-2}$	95	$4.67 \cdot 10^{-2}$	58
80	$6.42 \cdot 10^{-3}$	78	$5.75 \cdot 10^{-2}$	95	$5.05 \cdot 10^{-2}$	71
160	$3.70 \cdot 10^{-3}$	87	$5.76 \cdot 10^{-2}$	95	$5.31 \cdot 10^{-2}$	80
320	$2.10 \cdot 10^{-3}$	93	$5.76 \cdot 10^{-2}$	95	$5.46 \cdot 10^{-2}$	85
640	$1.23 \cdot 10^{-3}$	96	$5.76 \cdot 10^{-2}$	95	$5.54 \cdot 10^{-2}$	88

b)

s	$D_{gb,app}$ due to Hart-Mortlock's eq., nm^2/s	Error in % due to Hart-Mortlock's eq.	$D_{gb,app}$ due to Maxwell-Garnett's eq., nm^2/s	Error in % due to Maxwell-Garnett's eq.
5	$1.12 \cdot 10^{-2}$	62	$2.90 \cdot 10^{-2}$	2
10	$8.39 \cdot 10^{-3}$	72	$2.88 \cdot 10^{-2}$	2
20	$5.49 \cdot 10^{-3}$	81	$2.79 \cdot 10^{-2}$	5
40	$3.41 \cdot 10^{-3}$	88	$2.80 \cdot 10^{-2}$	5
80	$2.03 \cdot 10^{-3}$	93	$2.81 \cdot 10^{-2}$	5
160	$1.21 \cdot 10^{-3}$	96	$2.81 \cdot 10^{-2}$	5
320	$7.68 \cdot 10^{-4}$	97	$2.81 \cdot 10^{-2}$	5
640	$5.35 \cdot 10^{-4}$	98	$2.81 \cdot 10^{-2}$	5

Summary

The slope of the concentration profile ($\ln C_{av} = f(y^{6/5})$) increases as the average grain size decreases, and the grain boundaries orientations become important. Specifically, the ratio between the number of parallel and other diffusion paths is also very important in that sense. Accordingly, the slope also increases if the potion of parallel GBs is smaller than others. The increase of the slope suggests that D_{gb} can be underestimated when applying the conventional procedure, i.e. Le Claire's relation. Errors of the order of 50% are very possible (pure microstructure effect). The model of square grains, widely used in the literature, can represent an average microcrystalline structure, if the numbers of parallel and perpendicular diffusion paths are comparable. As the diffusion time grows, the role of perpendicular GBs vanishes, suggesting that the same criterion can be used for the transition from the B-regime to the A-regime for the models of square grains and parallel boundaries (for example, [Bel01]). In this case, the Hart-Mortlock equation is valid even for the model of square grains if the volume (area) fraction of GBs is calculated as for the model of parallel boundaries. However, segregation dictates new conditions for diffusion in polycrystalline materials. The diffusion profiles calculated for both models under these conditions differ, and the discrepancy increases with equilibrium segregation factors. The Maxwell-Garnett equation is not valid for the model of parallel boundaries, especially for large equilibrium segregation factors.